POLITECNICO DI MILANO

Scuola di Ingegneria Civile, Ambientale e Territoriale

Master of Engineering Science in Environmental and Land Planning
Engineering

CHARACTERIZATION OF THE GREEN ROOF GROWTH MEDIA

Supervisor: Prof. Chiara CORBARI

Co-supervisor: Prof. Denis M. O'CARROLL

Master Graduation Thesis by:

Ginevra A. PERELLI

MATRICOLA: 783495

Academic Year 2013 - 2014

Abstract

Green roofs are becoming a popular solution to manage the stormwater, to reduce the energy consumption in highly urbanized environment and provide many additional benefits. One of the key components that characterize the green roof system is the growth medium; the medium supports the plants, providing water and nutrient storage, and contributes to the roof insulation.

The object of this thesis is to investigate the hydraulic and the thermal properties of the green roof growth medium and to study the relationship among these properties through extensive laboratory analyses. In addition, the laboratory results are compared with direct measurements in the field, from the green roof site at the Western University campus. In the thesis is also analyzed an innovative methodology to indirectly estimate the soil water content and based on the thermal inertia approach. Despite the challenges posed by a complex soil such as the green roof media, the results presented in the thesis provide a detailed characterization and useful information that can be applied to understand and model the green roof system.

Keywords

Sommario

I Green Roof (o tetti verdi) sono una sempre più diffusa tecnologia adottata per gestire le acque piovane e ridurre i consumi energetici degli edifici, oltre a portare diversi altri vantaggi. Uno degli elementi chiave che caratterizzano il green roof è il terreno (growth media). Infatti, il g*rowth media* non solo provvede al sostentamento delle piante, offrendo acqua e nutrienti, ma contribuisce anche all'isolamento termico del tetto e costituisce l'elemento fondamentale per la mitigazione del *runoff*, riducendo e ritardando il picco di flusso dell'acqua piovana.

La tesi è stata svolta nell'ambito del Double Degree Program presso la Western University (London, ON, Canada), dove è anche collocato il green roof oggetto della ricerca. Il progetto di tesi è parte integrante del Green Roof Project, un progetto di ricerca che prevede lo studio estensivo dei green roof in diverse regioni climatiche del Canada. L'obiettivo specifico della tesi è di determinare le proprietà idrologiche e termiche del *growth media* e studiare le relazioni che intercorrono tra di esse, attraverso dettagliate analisi di laboratorio e sul campo. Infine, nella tesi viene anche considerata una nuova metodologia per la stima indiretta del contenuto idrico del suolo, basata sul concetto di inerzia termica. Nonostante le difficoltà incontrate nello studio di un terreno complesso ed eterogeneo come il tipo di *growth media* utilizzato, i risultati conseguiti offrono una dettagliata caratterizzazione ed informazioni utili per la comprensione delle prestazioni del green roof e l'implementazione del modello numerico elaborato all'interno del Green Roof Project.

Acknowledgments

First of all, as the thesis has been completed according to the Double Degree Program, I wish to express my deepest gratitude to my supervisors, Dr. Chiara Corbari, who provided valuable advices and support, especially during the final stage of my research, and Dr. Denis O'Carroll, who followed my work at Western University, helping me to develop an independent and critical approach.

I also would like to sincerely thank Dr. Chris Smart, Dr. James Voogt and Dr. Jason Gerhard for their helpful and constructive advices during my research and the assembling of the thesis.

Special thanks goes to the incredibly supportive Green Roof team and the Restore Group. In particular, to Dr. Maja Staniec who guided me through the initial steps of my master; her guidance and friendship helped me to quickly achieve confidence in my work.

Furthermore, this thesis would not have been possible without the tremendous encouragement of my family, who supported me along my thesis despite the distance. I also owe sincere thankfulness to my friends, the ones that supported me from my home country and the new ones, which I had the pleasure to meet at Western.

Last but not least, I would like to truly thank my boyfriend, Abhijit Saxena, for his support and help along my thesis and during the writing process, which would have been considerably longer without his valuable advices.

Table of Contents

List of Tables

List of Figures

List of Appendices

Glossary of Terms

Symbol	Definition	Units
q	Darcy's velocity	m/s
Q	Volumetric flow	cm^3/s
A	Cross sectional area of the soil chamber	cm^2
K, K$_S$	Saturated hydraulic conductivity	cm/sec
ΔH	Difference of hydraulic head	cm
ΔL	Distance	cm
i	Hydraulic gradient	-
P$_C$	Capillary pressure	cm of water
Pe	Entry pressure	cm of water
ψ	Suction	cm of water
S$_W$	Water saturation	-
Se	Effective water saturation	-
θ	Volumetric water content	-
θ_r	Residual volumetric water content	-
θ_s	Volumetric water content at saturation	-
d	Particle diameter	μm or mm
V$_T$	Total volume	cm^3

V_V	Volume of voids	cm^3
V_S	Volume of solids	cm^3
M_S	Dry mass of the solids	g
ϕ	Porosity	-
ρ_b	Bulk density	g/cm^3
ρ_S	Density of solids	g/cm^3
ρ_W	Density of water	g/cm^3
λ	Thermal conductivity	W/mK
λ_{dry}	Thermal conductivity for dry soil	W/mK
λ_{sat}	Thermal conductivity for saturated soil	W/mK
κ	Thermal diffusivity	m^2/s
C_V	Volumetric heat capacity	MJ/m^3K
T	Temperature	°C or K
Ke	Kersten number	-
P_C-S_W	Capillary pressure – saturation relationship	-
SWRC	Soil water retention curve	-
ADC	Analog digital converter	-
SH	Sailor and Hagos (model)	-
JH	Johansen (model)	-

CK	Côtè and Konrad (model)	-
LU	Lu et al. (model)	-
MV	Murray and Verhoef (model)	-

<div align="center">

Chapter 1

</div>

1 Introduction

Green roofs are becoming more and more popular solution for stormwater management in urbanized environments. They offer indeed several benefits, such as the reduction of the building energy consumption and the urban heat island effect. Moreover, green roofs can delay and reduce the runoff peak improving the quality of the stormwater. Green roofs also offer considerable advantage that they can be installed on unutilized surface areas (such as roof tops), which represent approximately 40-50% of the impermeable areas in cities [1].

Green roofs consist of a multilayer system and the focus of the thesis is on the substrate layer, or growth media, that supports the plants growth and provides the delay and reduction of the runoff peak.

The thesis is part of bigger project, the Green Roof Project that started in September 2012 at the Western University (London, ON). The project involves the study of three green roof sites, located in three different climatic regions of Canada: London (at Western University), Calgary (University of Calgary) and Halifax (Park Place V building) [2]. Data to determine the green roof energy and water balance have been collected continuously in each location till current date. LiveRoof [3] provided the growth media for the three green roof sites and the same type of medium is also used for the laboratory analyses described here.

Green roofs have been studied with several approaches based on direct field measurements or modeling. The second approach requires the knowledge of input parameters such as the soil physical properties. In the literature of the soil science, several studies on natural occurring soils or standard soils (such as clay silt or sand) are available. However, these studies cannot properly be applied on green roof modeling because green roof media are considerably different. They are indeed engineered lightweight soils that consist of several components, such as the aggregate and the organic matter. Nowadays,

more and more studies specifically based on green roof media are being published, expanding the knowledge in the field and the database of soil properties.

The thesis presents detailed analyses of hydraulic and thermal properties of fresh soil (never used on the roof) and used soil (used as growth media on the green roof in London). The analyses have been conducted in the laboratory and in the field. In Chapter 2 the challenges of studying the green roof media are discussed in detail. In the chapter the hydraulic and thermal properties of soils are discussed, focusing on the specific properties of growth media. In the thesis is also described an innovative approach to estimate the soil water content through the thermal inertia approach. Because of the dependency of the thermal properties on the water content, it is possible to correlate the thermal inertia of system to the water content. The approach is based on the acquisition of thermal in multispectral images and it was initially applied for large scale, using satellite platforms. Recently, the technology has started to be applied on smaller scale. The analyses conducted in the thesis represent one of the first applications of the methodologies on green roofs. In this early stage remote sensed images are not taken, however, the thermal inertia is calculated from direct measurements of thermal properties on the green roof. The laboratory results and the field measurements are then compared with the data collected on the three green roofs. Indeed, the measurements continuously collected at three sites offer an impressive database that represents an interesting why to compare the experimental analyses with the field experience.

1.1   Objective of the Thesis

The objective of the thesis is to characterize the hydraulic and thermal properties of the green roof growth media of the project and the relationships between them. This characterization aims to provide the input parameters for the numerical model of the project that will simulate the performances of the green roof. Moreover, the analyses of the soil properties and the comparison with the field data will offer a further understanding of the green roof.

Chapter 2 – Literature Review

2   Introduction

Green roofs (also referred as living roofs or eco roofs) are rooftops of buildings covered entirely or partially with a multilayer system of vegetation, substrate and impermeable cover. Green roofs can provide several benefits - some of which are related to the building itself, while other benefits can be appreciated when a larger number of green roofs are considered. Regarding the singular building, the installation of a green roof can provide the following advantages:

- It improves the building energy consumption by reducing the heat flux through the roof [4]. Indeed green roofs improve building insulation, reducing the need of sir conditioning in summer and heating in winter [5]. Regarding the cooling of the building, an important role is played by the vegetated layer. The shade provided by the plants reduces the surface temperature below the canopy, therefore less heat is transmitted to the building [6]. Moreover, through evapotranspiration (evaporation and transpiration combined) the plants can also cool the surrounding air, releasing water vapor and absorbing heat [6]. As a consequence, the decrease of the surface temperature reduces the heat flow into the building [6].

- Green roofs can prolong the useful lifespan of the roof, protecting the rooftop and mitigating extreme temperature changes from day to night and summer to winter [7] [8].

- It enhances the aesthetic appeal. Green elements in the urban environment provide a pleasant aesthetic element [7] [8].

The installation of many green roofs can provide the following benefits:

- They mitigate the heat island effect (phenomenon by which the temperature inside the city is higher than the surrounding temperature). The temperature reduction is due to the processes previously described; the plants through the

evapotranspiration absorb heat and release water vapor [8] [6]. In the same time, the heat flux from the roof to the atmosphere is reduced and the overall surface temperature on a green roof is colder than a normal roof [9].

- In some cases, green roofs can provide a friendly environment for those species that are usually disadvantaged in cities such as bees, butterflies, improving the biodiversity [5] [7] [9]. However, this benefit presents some restrictions. Nesting birds and chicks might be exposed to dangerous conditions, as for instance the lack water during long drainage period.

- They improve air quality [10]. Plants absorb carbon dioxide and capture air particles from urban pollution (particulate deposition) [7] [6].

- Most importantly, they help with storm water management. Green roofs can reduce and delay peak runoff from the rooftop, retaining some of the water in the layer system and releasing the excessive water later on. Green roofs can also improve runoff water quality [5] [8] [10].

Green roof systems can be classified into two main categories: intensive and extensive. Intensive green roofs are characterized by thicker substrate (100-200 mm) [10] and can support grasses, small bushes, perennial herbs [1] or large trees [6]. Extensive green roofs are shallower and can support only small plants (most commonly Sedum). This study will focus on the second type of green roof.

Green roofs are made of different layers (as shown in Figure 2.1) which can vary from one design to another. Typically, the main layers consists of the followings:

- Vegetated layer: plants, through the transpiration, cool the surrounding atmosphere and restore the water capacity of the substrate (up taking the water from the soil though the roots). Vegetation also intercepts the precipitation and the roots improve soil permeability and compaction. During the summer, the shadow of the canopy helps to reduce the temperature [10].

- Growth media (or substrate layer): it represents the support for the vegetated layer and provides storage of nutrients and water. The substrate is crucial to stormwater management of the green roof, providing water storage and extending the path of stormwater in the system [10].

- Drainage layer: a coarse aggregate material that allows the rapid drainage of the excessive stormwater [10].

- Waterproofing layer: an impermeable layer designed to protect the roof. It can also include a root barrier layer as additional protection.

Vegetation

Substrate

Drainage layer overlain with filter fabric

Waterproofing membrane/ Root barrier

Roof Surface

Figure 2.1: Main layers of a green roof (reproduced from [10]).

The thesis will focus on the substrate layer (the growth media) and its physical properties. Green roof media are engineered lightweight soils and are very different from natural occurring soils. Since the design of a green roof depends on the climate and the availability of materials, there is not a universal growth medium [11]. A typical growth medium for green roofs usually consists of three main components: aggregate (a porous light weight material), sand and organic matter. The composition of the growth medium strongly depends on local availability and cost of the materials [12]. The most common types of aggregate in Europe and North America are expanded slate (typically used in the

eastern US), expanded clay (commonly used in the mid-western and eastern US) and expanded shale (mostly in western US) [12] [13]. The expanded shale is an engineered lightweight material characterized by high porosity and which commonly used as a substrate for plants growth or in the construction industry [14]. In order to create these characteristics (light weight and high porosity), the shale (a natural sedimentary rock) is heated with a controlled-temperature process (between 100 and 150°C), during which the material expands. Therefore, the final result of the process is the expanded shale [14]. Expanded clay and expanded slate are generated with a similar process. In the UK heavier aggregate are generally used such as crushed brick, while In New Zealand and in the North-West Pacific area volcanic materials are more common (such as pumice and zeolite) [13]. Volcanic materials are convenient for green roof substrate due to the high porosity (high water storage capacity) and light weight [7]. The aggregate usually ranges from 50 to 80% by volume and the organic matter (compost) can vary from 10 to 20% by volume (the fraction is, generally, preferred between 0 to 10% because the higher the organic content the more the substrate is likely to lose volume over time). High lignin compost (as peat, bark, yard waste and recycled paper) is a preferred alternative to compost [7].

2.1   Challenge of Green Roof Growing Media

Growth media designed for green roofs, as previously discussed, are heterogeneous mixtures of inorganic and organic material with particles of different grain sizes. These media substantially differ from natural occurring soils as they include artificial components (e.g., expanded lightweight materials). The literature regarding soil science offers detailed and extensive studies about natural soils and standard materials (such as sand, clay, sandy loam, etc.) while for green roofs there is still little information [12].

There are different approaches to study and quantify green roof performance; some of them are based on field measurements while others on modeling [12]. Both approaches require the knowledge of soil properties; in particular models need data as input parameters. Most important, it is necessary to know the thermal properties and their dependency on moisture content in order to describe the heat transfer and storage through

the soil [12]. Finding these properties for growth media could be challenging, especially due to the presence of clay, expanded lightweight material and organic matter (bark and peat). As it will be discussed in Chapter 3, some of the methodologies, developed for natural or standard soils, required adjustments or modifications in order to be applied on green roof growth media.

2.2   Soil Hydraulic Properties

The hydraulic properties of the media directly impact the stormwater management performance of the green roof. The hydraulic properties can be divided into two categories of soil conditions: saturated and unsaturated soil. In these two conditions, the porous media presents different characteristics and behaviors.

2.2.1   Saturated Soil

When the soil is fully saturated, all the pores are filled with water. The one-dimensional flow, through the porous media, follows the Darcy's Law for saturated soil [15] [16] (the water flow through unsaturated soils is discussed in the next paragraph):

$$q = \frac{Q}{A} = -K\frac{\Delta H}{\Delta L} = -Ki \qquad 2.1$$

where q represents the Darcy's Velocity (cm/sec), Q is the volumetric flow (cm^3/sec) and A represents the cross-sectional area (cm^2) of the portion of medium considered. K is the saturated hydraulic conductivity (cm/sec) that indicates the facility with which water (generally any fluid) flows through a saturated porous medium. The hydraulic gradient, i, is the driving force of the water flow through the soil, calculated as the difference of the total hydraulic head (ΔH, usually simply referred as "head") between two points and divided by the length in between (ΔL) [15] [16]. The total potential energy (or hydraulic head), H, in saturated soil, is given by the sum of the elevation head (Z) and the pressure head (p/ρ_wg); where p represents the pressure, ρ_w represents the density of water and g represents the gravitational acceleration [15] [16]. The pressure head at the air/water interface in the ground is considered zero (the pressure head at the water table is zero).

Hydraulic conductivity is an important property. First, when the green roof has reached the maximum holding capacity (i.e. when the soil is not able to hold more water against the gravity pull) during a rainfall event, the excess rainfall should flow through the media without ponding [13]. Good soil permeability is therefore a key factor for the green roof stormwater management. Ponding should be avoided because it increase the structural load on the roof top and can generate surface runoff which contributes to the erosion from the green roof. Moreover, the generation of runoff considerably reduces the positive effect of the green roof, in terms of peak flow attenuation [13].

There are several methods to calculate K: field and laboratory based [16]. Among the laboratory methodologies, there are two main categories: the *falling head* method and the *constant head* method. With the falling head method, the soil sample is initially saturated under a certain head and then the water is allowed to flow out. With the constant head method, the water flows through a saturated soil sample with a constant head condition applied on the specimen. The volumetric outflow, Q, from the specimen is recorded over a period of time. Knowing Q, L and A (the length and the cross-sectional area of the sample), t (time in which the flow fills a certain volume) and the applied head (H), it is possible to calculate K using Darcy's Law (eq. 2.1).

The hydraulic conductivity of soils can range from 10^{-9} cm/sec (for clay) to 10^{1} cm/sec (for gravel) [16]. According to the FLL guideline (the worldwide accepted German guideline for green roof standards [17]) the minimum (saturated) hydraulic conductivity for extensive green roof should be 0.001 cm/sec. Values of hydraulic conductivity for different green roof substrates are also available in the literature. Table 2.1 reports the values of the saturated hydraulic conductivity from several green roof studies for different substrates. Substrate made of volcanic materials (as pumice, lapillus and zeolite) present a high hydraulic conductivity (compared with the minimum value suggested by the FLL guide line), as for Palla et al. in [18] [19], Fassman in [13] [20] and for Corbari in [21]. It has to be noted that in [13] [20] only the soil tested in the laboratory had a high hydraulic conductivity, while the substrate used for the construction of the green roof (bulk blended) had a higher content of fine particles (as specified by the authors) and presented lower values for K. The substrate tested in [22], made of crushed bricks,

presented a high hydraulic conductivity. Substrates with a medium-high content of organic matter (compost, peat, bark) generally presented lower hydraulic conductivity, as for [23] and [24]. In Table 2.1 higher porosity generally corresponds to higher hydraulic conductivity. Finally, the content of fine particles can influence the hydraulic conductivity.

Table 2.1: Substrates and properties for different (extensive) green roof studies. (*)
***L.* refers to the soil utilized in the laboratory experiments while *B.* refers to the soil**
provided for the construction of green roof that had a higher content of fines.

Study	Growth Medium/a	ρb (g/cm3)	ϕ	K (cm/sec)
Palla et al. 2009 (Italy) [18] [19]	Lapillus and Vulcaflor, mixed soil (lapillus,pumice, zeolite, peat)	Lapillus: 0.984 Vulcaflor: 0.936 (measured)	Lapillus: 0.65 Vulcaflor: 0.65 (measured)	Lapillus: 0.33 Vulcaflor: 0.08
Nagase and Dunnet	Substrate based on crushed tile/brick	0.94-0.98	0.63-0.64	0.1
Babilis and Londra (Greece) [??]	Compost 70%, pumice 30% Compost 70%, til gravel 30%l	0.388 20.588 (Measured)	-	0.0348 0.0335 (Measured)
Fassman et al. (New Zealand)	Pumice 80%, composted bark 20% Pumice 40%, expanded clay	0.99 0.89	0.59 -	0.005 0.034
Fassman and Simcock [13] Fassman	-Pumice (Lab. and Bulk blended)* -Zeolite (Lab. and Bulk blended)	Pumice: L. 0.594, B. 0.989 Zeolite: L. 0.598, B. 0.857	-	Pumice: L.0.101, B.0.005 Zeolite: L.0.096,
Bond and Thompson (New	50% pumice, 35% sand, remaining silt and finer particles.	0.59	0.59	0.04

DeNardo et al. (Pennsylvania) [26]	12.5% sphagnum peat moss, 12.5% coconut fiber, 15% perlite, 60% hydrolite	-	0.553 (measured)	1.26 (estimated)
Corbari and [21] (Italy)	Lapillus and expanded perlite	-	-	0.126 (measured)
FLL Guideline	Substrate for extensive green roofs	-	-	>0.001

2.2.2 Unsaturated Soil

Saturated conditions are generally rare for green roofs, unless after a prolonged rainfall event. In most cases, the soil is generally unsaturated, with the pores partially filled with air and water. For this reason, it is important to understand and model the soil behavior in these conditions. Indeed, the infiltration (the flow of the rainwater through the soil [27]) and the water retention are fundamental processes that characterize the stormwater management performances of the green roof.

In the unsaturated soil the Darcy's law that was previously discussed, is no longer applicable to describe the flow through the media. Indeed, in unsaturated soils the hydraulic conductivity depends on the water content [23]. However, the Darcy's law can be rewritten as the Darcy-Buckingham equation, where the hydraulic conductivity is expressed as function of the water content (θ) or the soil suction ((ψ) [25] [19]. Here follows the equation for one dimension:

$$q_z = K(\theta)\frac{\partial h}{\partial z}$$
2.2

the combination of the Darcy-Buckingham equation and the continuity equation, the Richards equation can be written as follows [25] [19]:

$$\frac{\partial \vartheta(\psi)}{\partial t} = \frac{\partial}{\partial z}\left[K(\psi) \cdot \left(\frac{\partial P_C}{\partial z} + 1\right)\right]$$
2.3

eq. 2.3 represents the flow in one dimension (z), i.e. the vertical flow from the soil surface into the substrates layers during the infiltration process. The suction (ψ) represents the negative pressure exerted on the water by the soil matrix. In soil science ψ is also referred as *matric potential* or *capillary potential* and is a function of the volumetric water content θ (V_w/V_v) [28]. When the water flows into the soil, the moisture content increases and the suction decreases [13].

The relationship between the moisture content and the matric potential is a characteristic of the soil and is usually referred as *soil water retention curve* (SWRC) or *soil water characteristic curve* [28] [29]. The water content can be expressed as volumetric water content (θ) or degree of saturation (S_w) [30], which is calculated as the volumetric water content divided by the soil porosity. In the thesis the relationship is noted as $P_C - S_W$. Where P_C is the capillary pressure and represents the absolute value of the suction ($P_C = |\psi|$).

Studying the SWRC is fundamental for assessing green roof hydrologic performances. The ability of the soil to retain and store the water directly affects the active storage of the rainfall during a storm event [13]. For instance, the maximum amount of rainfall that can be stored (i.e. the volume of the peak flow reduction) represents the maximum amount of water that the soil can retain against the gravity pull, defined as field capacity. The field capacity can be derived from the SWRC [13]. Moreover, the quantity of the water that a substrate can store, influences the sustainment of the plants, which are usually not irrigated (in case of extensive green roof). The water storage also impacts the evapotranspiration process of the green roof [13]. The wilting point represents that level of soil suction (or capillary pressure) after which plants are not able to extract water from the soil, because it is held with too strong forces, and start to wilt [13]. The characteristics of the $P_C - S_W$ are discussed in more detail in the following paragraph.

2.2.2.1   Soil Water Retention Curve (SWRC)

The $P_C - S_W$ relationship depends on many soil characteristics such as composition, organic content [31], texture and grain size distribution. The relationship is defined by two boundary curves as illustrated in Figure 2.2: the drainage and imbibition (or wetting)

curves. These two curves are not the same due to hysteresis [30]. For the same reason, there are infinite loops of the same curves between the two boundary curves that are different from each other. Different pathways are followed when water saturates or drains out of the porous media. Droplets of water or air bubbles can remain trapped in the pores and can change the pores availability in the soil matrix. Any curve can be studied starting from any level of saturation and the increase or decrease of saturation generates one of the two curves (drainage or imbibition).
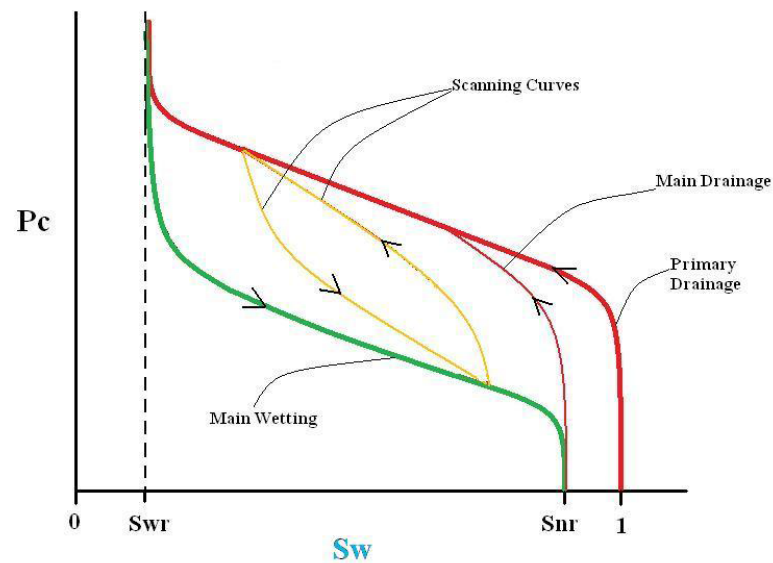
Figure 2.2: The two boundary curves of the P_C-S_W relationship and its loops (scanning curves). S_{Wr} represents the residual water saturation, the amount of water that cannot be physically displaced by air (reproduced from [32]).

The curve that describes the soil drainage from saturated condition (S_W =1) is referred to as the *primary drainage curve* and represents one of the two boundary curves of the $P_C - S_W$ relationship. In the same way, the curve that describes the soil wetting from dry condition (S_W =0) is named Primary Imbibition Curve. The green curve in Figure 2.2 indicates the *Main Wetting* curve that describes the imbibition when the soil contains only the residual water content.

2.2.2.2 Characterization of the unsaturated soil properties

The most common methods to measure the SWRC are pressure plate or Tempe Cell methods [29]. Other methods include the filter paper technique, the hanging column method and different types of tensiometers [30] [29]. Direct measurements of the SWRC are usually time consuming [30] [29] and for this reason scientists have also developed indirect methods and empirical models to describe the SWRC as in [33] [34] [35] [36]. As the authors in [28] report, Brooks and Corey proposed in 1966 an empirical formulation that relates the water content to the soil capillary pressure:

$$Se = \left[\frac{P_c}{P_e}\right]^{-\lambda} \qquad\qquad 2.4$$

Where Se is the effective saturation and it is defined as:

$$Se = S_e = (\theta - \theta_r)/(\theta_s - \theta_r) \qquad\qquad 2.5$$

where θ_r and θ_s are respectively the residual and saturated water content. The parameter λ in eq. 2.4 is experimentally derived and it is related to the soil size distribution index [33]; Pe represents the entry pressure, the critical pressure that air has to exceed to invade the largest pores to displace water.

Van Genuchten (1980 proposed an empirical relationship [28]:

$$\theta(Pc) = \theta_r + \frac{(\theta_s - \theta_r)}{[1 + (a|Pc|)^n]^{1 - 1/n}} \qquad\qquad 2.6$$

where a and n are empirical parameters. The parameter a (cm^{-1}) is related to the inverse of the entry pressure (Pe) and it is greater than zero; n (dimensionless) refers to the pore size distribution and it is greater than unity [28].

Table of values for a and n, for different types of soils, are available in the literature as reported in [33] [36] [34] [35]. These studies report values for standard categories of soils, such as sand, loam, silt loam, clay etc. that are different from green roof growth media. However, some green roof substrates can be modeled as a one of the soil type

listed in the tables. For instance, in [18] the authors modeled two green roof substrates as standard soils: the Vulcaflor substrate was considered as loamy sand with a=0.124 cm^{-1} and n = 2.28; the second substrate, Lapillus, was considered as coarse sand with a=0.079 cm^{-1} and n=6.97. In [19] the authors considered the growing medium as sand loam (a=0.075 cm^{-1} and n=1.89) and the drainage substrate as sand (a = 0.145 cm^{-1} and n= 2.68). In another study [25], *a* and *n* were 0.8 cm^{-1} and 1.5, respectively, for the substrate (that is more similar to the type used for this thesis). In [27]and [37], the authors used sand and loam instead of green roof media for the physical experiments.

As earlier discussed, in addition to the soil water retention relationship, the infiltration through the unsaturated media represents a fundamental component to model the green roof hydrology. However, the measurements of the unsaturated hydraulic conductivity are generally difficult and time-consuming; therefore, scientists have developed models to estimate it from the soil water retention curve and the saturated hydraulic conductivity K [23]. Regarding the green roof studies, a common method is to utilize the Richard's equation (2.3) combined with the Van Genuchten-Maulem relationship, as described in [18] [25], where K(θ) is related to the saturated hydraulic conductivity (here noted as K$_S$) and to the water content, which is also related to the soil water retention curve as follows:

$$
\begin{cases}
\theta(P_C) = \theta_r + \dfrac{\theta_s - \theta_r}{[1 + |\alpha P_C|^n]^m} \\
K(\theta) = K_S S_e{}^{0.5} \left[1 - \left(1 - S_e{}^{1/m}\right)^m\right]^2
\end{cases}
\qquad 2.7
$$

For instance, this method is used in the numerical models HYDRUS-1D applied in [25] [38] [19] and SWMS_2D in [18] for the green roof hydrological simulation.

2.3 Thermal Properties

Thermal properties of soil are needed to describe the distribution of the energy and the heat transfer in the soil [39] [40]. They are also essential to analyze green roof systems and the energy balance of the roof [8]. The heat transfer through the soil is a complex phenomenon. It depends on various physical properties and the moisture content of the media. The physical processes consist of the following:

- Conduction: it occurs through the soil particles (grains) and liquid (water is utilized for the experiments) [41];

- Latent heat transfer: it occurs through evaporation and condensation cycles [41];

- Sensible heat transfer through vapor and liquid diffusion and convection [41];

- Radiation: it can occur in air filled pores [41].

The heat transfer by conduction is usually the predominant process for what concerns the substrate layers [41]. The one-dimensional equation that describes the conduction though the soil in one dimension is described by the following equation as reported in [42]:

$$G = -\lambda \frac{\partial T}{\partial z} \qquad\qquad 2.8$$

where G represents the heat flux through the media (W/m^2), $\frac{\partial T}{\partial z}$ the temperature gradient through the vertical direction z (the temperature gradient can be expressed with the units K/m) and λ is the thermal conductivity (W/mK) and it describes the ability of the material to conduct heat [43].

The other important thermal property of interest, when studying the green roof thermal behavior, is the volumetric heat capacity C_V, which represents the heat storage in the media. Heat capacity and thermal conductivity are connected to each other through the following equation [42]:

$$\kappa = \frac{\lambda}{C_V} \qquad\qquad 2.9$$

Where κ is the soil thermal diffusivity (m^2/s).

Thermal properties depend on many factors; such as the soil texture, mineralogical composition [41] [44] [45], organic content, and above all, the water content [44] [41]. As reported in [45] and [43], the thermal conductivity also varies with bulk density (ρ_b) which is the measure of the compaction of the medium. With the increase in the compaction of the soil, the bulk density (given as $\rho b = M_S/V_T$) increases and the porosity reduces. It also increases the contact between the soil grains improving the heat conduction, the main process for the heat transfer. As mentioned earlier, the thermal conductivity is strongly affected by the water content in the soil [40] [41] [43] [44] [45]. At 20°C, the thermal conductivity of air (0.025 W/mK) is one order smaller than the conductivity of water (0.596 W/mK) and two orders smaller than solids (2.5 W/mK). Therefore, as the water content increases in the porous medium, it replaces air, which results in increasing the thermal conductivity of the soil [39]

2.3.1   Measuring and Modeling Thermal Properties in Soil

The authors in [39] and [46] reported that Kersten conducted one of the first experimental studies on the thermal properties in 1949. For instance, the thermal conductivity is calculated with empirical formula as reported in [47]:

$$\lambda = 0.1442(a_1 log\theta - a_2)10^{a_3 \rho_b} \qquad\qquad 2.10$$

where a_1, a_2 and a_3 empirical constants (dimensionless)

As cited in [48] De Vries proposed two other methods to estimate the thermal conductivity and the volumetric heat capacity. The volumetric heat capacity is calculated as the weighted sum of the volumetric heat capacity of the components of the soil as follows:

$$C_V = C_{Vm}\chi_m + C_{Vo}\chi_o + C_{Vw}\chi_w + C_{Va}\chi_a \qquad\qquad 2.11$$

where χ represent the volumetric fraction of the component and the subscripts *m, o, w* and *a,* indicate respectively the content of minerals, organic matter, water and air. If the mineral and organic content are grouped into one volumetric fraction, the solids, and if the contribution of air is neglected, eq. 2.11 can be rewritten according to the Campbell equation as reported in [39] [48]:

$$C_V = \chi_s C_{Vs} + \chi_w C_{Vw} \qquad 2.12$$

Eq. 2.12 shows the direct dependence of the heat capacity on the volumetric water content and the equation can be also written as [48]:

$$C_V = (1 - \phi)C_{Vs} + \theta C_{Vw} \qquad 2.13$$

The volumetric heat capacity can also be calculated as follows [42]:

$$C_V = \frac{2.01{\times}10^6{\times}\rho_b}{2.65} + 4.19{\times}10^6 \theta \qquad 2.14$$

The equation can be applied to a soil with a negligible amount of organic content and a particle density of 2.65 g/cm^3.

Regarding the thermal conductivity, a commonly used formula is the one proposed by De Vries and reported in [39] [46]. The formula is based on the thermal conductivity of the soil component according to their volumetric fractions:

$$\lambda = \frac{\sum_{i=0}^n k_i \lambda_i \chi_i}{\sum_{i=0}^n k_i \chi_i} \qquad 2.15$$

where k_i depends on the shape and the arrangement of the soil particles and is calculated as follows:

$$k_i = \frac{1}{3} \sum_{i=1}^n \left[1 + \left(\frac{\lambda_i}{\lambda_0} + 1 \right) g_i \right]^{-1} \qquad 2.16$$

where *g* represents the shape factor. The subscript *0* refers to the fluid around the soil particles, which can be air in case of dry soil, or water for moist soil (k$_0$ =1).

Besides empirical formulations, the accuracy in measuring thermal properties has largely benefitted from technological progress. In particular the introduction of the heat pulse technique, pioneered by Bristow (as cited in [46]) allowed the simultaneous measurements of all the three thermal properties (λ, C_V and κ). In this way, the thermal properties can be indirectly measured through the increase or decrease of temperature in response to a heat pulse from a line source (the needle of the probe) [4].

2.3.2   Thermal Properties of Green roof Growth Media

As reported in [7] [12] [43] [49], previous studies have proposed models to relate thermal properties, in particular λ, to the moisture content, usually expressed as volumetric water content (θ) (e.g., Kersten in 1949, De Vries in 1963, Johansen in 1975, Campbell in 1985 and Côtè and Konrad in 2005). The empirical model proposed by Kersten (eq. 2.10) is based on laboratory measurements and the bulk density is required as an input parameter; however, it does not include soil mineral composition [49]. According to the authors in [12], the model does not provide an accurate representation of the soil properties at low water content, which is usually critical for green roof modeling. Côtè and Konrad, in [49], also stated that the Kersten model is only applicable for fine textured soil and sands. According to [49], the model developed by De Vires (eq. 2.15 and 2.16), which is physically based, considers mineral composition; however, as pointed in [43], it requires an accurate determination of various soil parameters. Similarly, as reported in [43], in the empirical model proposed by Campbell, λ is expressed as a function of θ and requires five soil parameters, which are often hard to define for green roofs.

As reported in [12] [43] [49], Johansen introduced a novel concept, the normalized thermal conductivity. Johansen proposed a simple empirical model, based on the non-dimensional water saturation (S_W) and mineral composition. The thermal conductivity increases from dry soil to saturated soil [12].

$$\lambda = \left(\lambda_{sat-dry}\right)Ke + \lambda_{dry} \qquad 2.17$$

Ke represents the Kersten number and is determined as follows:

$$Ke = 0.7 log Sw + 1.0 \qquad\qquad 2.18$$

The model accurately predicts the thermal conductivity for fine textured soil and sands; however, in order to consider a wider range of soil types such as natural soils, Côtè and Konrad in [49] proposed an improvement of the Johansen model and analyzed many test results available in the literature. As reported in [12], the improved model proposed by Côtè and Konrad introduced a soil textural parameter (*h*) for the Kersten number calculation:

$$Ke = \frac{hSw}{(1 + (h-1)\,Sw)} \qquad\qquad 2.19$$

Where *h* is equal to 4.6 for gravel and coarse sand and 0.6 for organic fibrous solids. According to Sailor and Hagos in [12], the model is not accurate at low water content and fine textured soils. In [43], the authors proposed another model to determine the Kersten number:

$$Ke = e^{[\alpha(1 - Sw^{(\alpha - 1.33)})]} \qquad\qquad 2.20$$

where $\alpha = 0.96$ for coarse textured soils and $\alpha = 0.27$ for fine textured soils [12].

As pointed in [12], all the models previously described, as many other studies on soil thermal properties, have been designed for standard soil such as sand, sandy loam, clay loam, silt loam [39] [40] [43] [45]. It is noted that the model proposed by Côtè and Konrad in [49] included natural soils and construction soils. However, there is an apparent lack of studies on green roof growth media. As mentioned before, growth media are different from natural occurring soil and even more so from standard and homogenous materials; therefore, literature models cannot accurately predict thermal parameters in a green roof system [7]. The authors in [7] reported one of the first extensive studies on green roof growth media in 2007. In this study, the authors analyzed the thermal properties over different moisture contents for eight types of green roof growth media common in the U.S. The authors concluded that the thermal property data of naturally occurring soils are not representative of green roof soils. An extension to the

work presented in [7], was reported in [12] in which 12 samples of green roofs soil with different composition have been characterized. According to the study, thermal properties vary significantly not only with moisture content but also with the type of growth medium. Therefore, it is important to quantify different growth media thermal properties. In [12], the authors proposed a model (eq. 2.13) to correlate thermal conductivity and water saturation (S_W) and compared it with the models available in the literature for naturally occurring soils (presented earlier in this chapter). The authors proposed a simple model relating a non-dimensional thermal conductivity (λ/λ_{dry}) with the water saturation (S_W):

$$\frac{\lambda}{\lambda_{dry}} = \frac{1.45e^{(4.411Sw)}}{1 + 0.45e^{(4.411Sw)}} \qquad 2.21$$

The authors concluded that the relationship between λ/λ_{dry} and S_W shows an exponential trend and the models proposed by Johansen, Côtè and Konrad, and Lu et al. (previously discussed) seem to overestimate the thermal conductivity, particularly for low water saturation levels [12].

Regarding the range of values for the green roof thermal conductivity, some information can be found in the literature. However, there is still a limited availability of useful data for green roof modeling [50]. As discussed before, the most extensive studies were conducted by [7] and [12], in which different green roof substrates were analyzed under different conditions of moisture content and soil composition. In [7] the authors studied two types of aggregate: expanded shale and pumice. They found that the aggregate, based on expanded shale, had a higher thermal conductivity than the pumice; the opposite was found for the heat capacity. Moreover, the authors reported that the increase of the aggregate and organic fractions equally reduces the thermal conductivity in dry soil.

In the second study [12], which continues the study presented in [7], the authors tested 12 different green roof soils. The aggregate consisted of three types: porous silica, expanded shale or expanded clay. Each aggregate was combined with sand and organic matter at different volumetric fractions. According to the results, the authors observed that the thermal conductivity is strongly affected by soil composition, followed by the thermal

diffusivity, while the heat capacity presented a moderate variability. The difference between the variability between thermal conductivity and heat capacity is also visible from Figure 2.3. The authors report that the soil based on porous silica presented the lowest thermal conductivity, while the soil based on expanded slate had the highest. As a general behavior, the differences from one type of soil to another were more consistent at higher water contents. In the study, in agreement with [7], increase in organic content resulted in a decrease in the thermal conductivity. The authors also underline the linear relationship between the thermal conductivity and the bulk density. Figure 2.3 shows the results regarding the thermal conductivity and the heat capacity in relation to the volumetric water content.
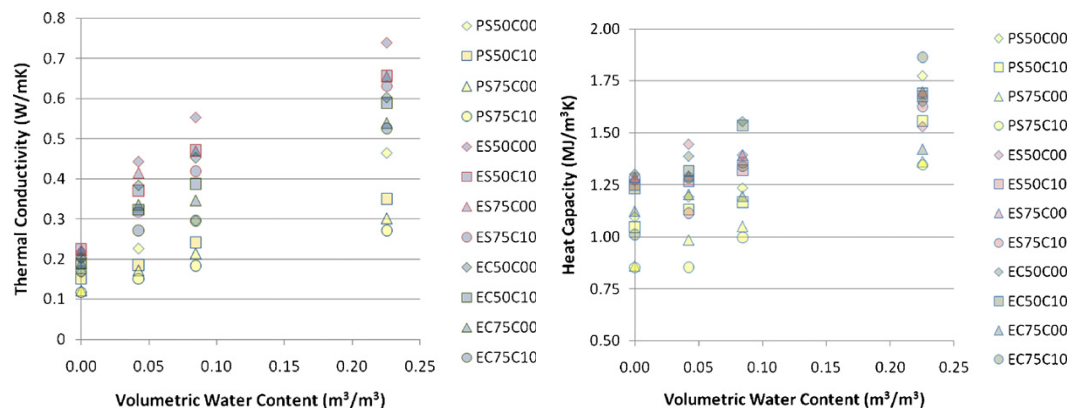
Figure 2.3: Thermal conductivity and heat capacity in relation with the water content for 12 green roof media (reproduced from [12]). The legend on the right indicates the type of samples. The initial letters indicate the name of the aggregate, followed by its volumetric fraction (50 or 75) and the organic content (C0 or C10).

In another study [8], the authors analyzed five different green roof substrates that are characterized by a high porosity and organic content (Figure 2.4).
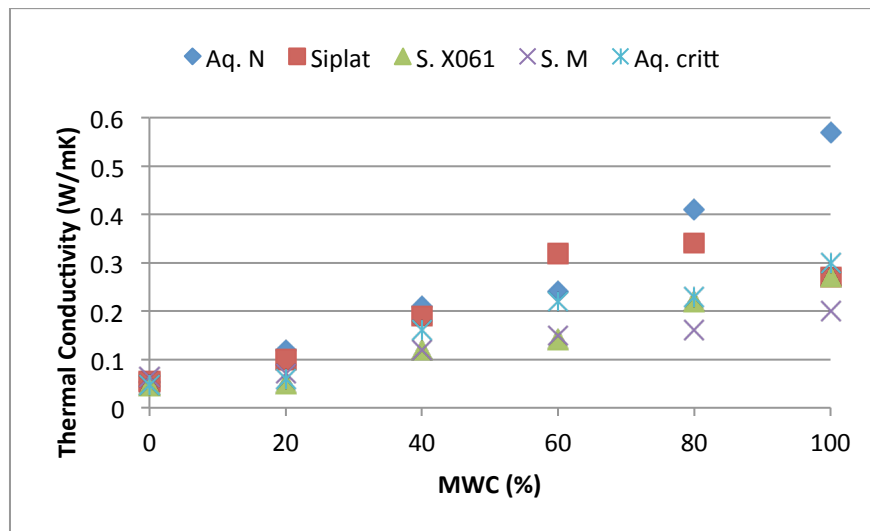
Figure 2.4: Thermal conductivity for five different substrates (reproduced from [8]) in relation with the water content.

As shown in Figure 2.4, the thermal conductivity increases always linearly with the moisture content; however, the range of values of λ is lower than the one reported in the other two studies above reported. This can be explained because the five substrates have a higher porosity that reduces the contact between particles, and a higher organic content. As stated in the studies previously discussed, the differences between substrate types increases with the moisture content; as shown in Figure 2.4, for dry soil, all the five substrates present almost the same thermal conductivity.

2.3.3 Estimation of the Soil Water Content with the Thermal Inertia Approach

In the previous paragraph the models that describe the relationship between thermal properties and water content have been discussed. This paragraph presents an alternative approach to indirectly estimate the water content from the thermal properties. The method is based on the remote sensing techniques that use the visible (VIS), near-infrared (NIR) and thermo-infrared (TIR) regions of the electromagnetic spectrum [51]. The technique has been initially applied on large-scale analyses from satellite platforms; however, with the recent availability of multispectral camera (for the VIS-NIR region) and thermal camera (for TIR), the approach started to be applied on the local scale [52].

The studies presented in [53] [51] [54] are indeed based on laboratory analyses on standard soils. The local scale can also include the green roof field. For instance, the method is currently investigated on the extensive green roof at the University Politecnico di Milano [55].

The remote sensing imaging technologies are based on the concept of thermal inertia, P (J/m^{2}Ksec$^{1/2}$) that represents the response speed to a temperature change in terms of energy flux. The thermal inertia is calculated as [53] [51]:

$$P = \sqrt{\lambda \rho C} \qquad \qquad 2.22$$

where λ is the thermal conductivity (W/mK or J/smK), ρ represents the bulk density (kg/m^3) of the wet soil and C the specific heat (J/kgK). The equation can also be rewritten as:

$$P = \sqrt{\lambda \rho C_V} \qquad \qquad 2.23$$

where C_V is the volumetric heat capacity (J/m^{3}K). Models that relate the thermal conductivity to the water content have been discussed in the previous paragraph. In addition to these models, the authors in [53] [51] describe the models proposed by Murray and Verhoef [54] and Lu et al. [56] that relate the thermal inertia and the soil moisture content. Similarly to the model proposed by Johansen (eq. 2.17), the thermal inertia is calculated as follows:

$$P = K_P (P_{SAT} - P_{DRY}) + P_{DRY} \qquad \qquad 2.24$$

Where P_{SAT} and P_{DRY} are respectively the thermal inertia for saturated and dry soil. K_P is the modified Kersten function, expressed as [51] [54]:

$$K_P = exp\left[\varepsilon\left(1 - \left(\frac{\theta}{\phi}\right)^{-\mu}\right)\right] \qquad \qquad 2.25$$

Where ε and μ are soil parameters, respectively equal to 0.6 and 0.71 for fine textured soils; 2.95 and 0.16 for coarse textured soils. The water content can then be estimated from eq. 2.25 as follows [51]:

$$\theta = \phi \left(1 - \frac{lnK_P}{\varepsilon} \right)^{1/-\mu} \qquad \text{2.26}$$

And, with the independent measurements of the thermal inertia, K_P can be calculated as [51]:

$$K_P = \frac{P - P_{DRY}}{P_{SAT} - P_{DRY}} \qquad \text{2.27}$$

Chapter 3 – Materials and Methods

3   Introduction

This chapter describes the methodologies and materials used in the thesis to determine the physical properties of the growth media. As discussed in Chapter 2, characterizing the physical properties of green roof media is challenging. It was observed that the conventional methods to characterize the natural and standard soil properties didn't adequately apply to green roof media. For this reason, some of these methods have been modified to adapt to the new material. The adapted methods have been initially tested on standard materials (a coarse silica sand, Unimin Corp.) in order to verify the consistency of the new methods. The results of sand can be compared with the results of previous studies in the literature (Appendix B).

In the thesis, every experiment was conducted at room temperature (21°C ± 2°C) and the water utilized was de-ionized (D.I) water.

3.1   Green Roof Growing Media

LiveRoof [3] provided the growth media utilized for the three green roofs of the project and the laboratory analyses presented in the thesis are conducted on the same soil in order to allow the comparison with the field data. The comparison is important to understand the behavior and the rate of change of soil properties over time. As the growth media are exposed to the outdoor environment and support plants growth, some of the soil physical properties (such as the organic content and the soil composition) are likely to change. Therefore, for the laboratory analyses, two types of soil were tested: *fresh* or *old* (or used). The fresh soil refers to the growth media that never supported plants and was never exposed to the outdoor environment. On the other hand, the *old* soil refers to the growth medium taken from the green roof site in London (Ontario). The *old* medium consisted of one-year old module, vegetated with sedum. The plants and the roots have been removed and the module was divided into 9 sections: the surface was divided into three rows which are then divided into three layers along the depth of the module.

As discussed in Chapter 2, green roof soils typically consist of three major components: lightweight aggregate, sand and organic matter. The lightweight aggregate for this growth media is a type of expanded shale (coarse and fine) that represents more than 50% by volume of the soil. This material provides high porosity, good water holding capacity and good thermal insulation (refer to [57] for more information). The organic matter, approximately 25% by volume, consists of bark and peat moss. It provides a strong water holding capacity because of the high porosity. The remaining components, sand, a pH buffering material (limestone) and expanded clay, adds additional water holding capacity to the soil and increases the porosity. It is also capable of absorbing water and storing nutrients for plants.

3.2   Materials

3.2.1   Pressure Cell

The main set up, on which most of the laboratory analyses are conducted, is a custom-built cylindrical aluminum pressure cell (illustrated in Figure 3.1). It is 20 cm long and has an internal diameter of 10 cm. The column has ports along its length to install three sets of $P_C - S_W$ measurement instruments. Each set consists of one soil moisture sensor, EC-5 (Decagon Devices, WA, USA) and one wetting phase tensiometer that is connected to a pressure transducer. Each set is installed at 7, 10 and 13 cm from the top of the column. Figure 3.2 shows the cross sectional view of the column. This set up was previously used in other studies, reported in [32], [58], [59] and [60].
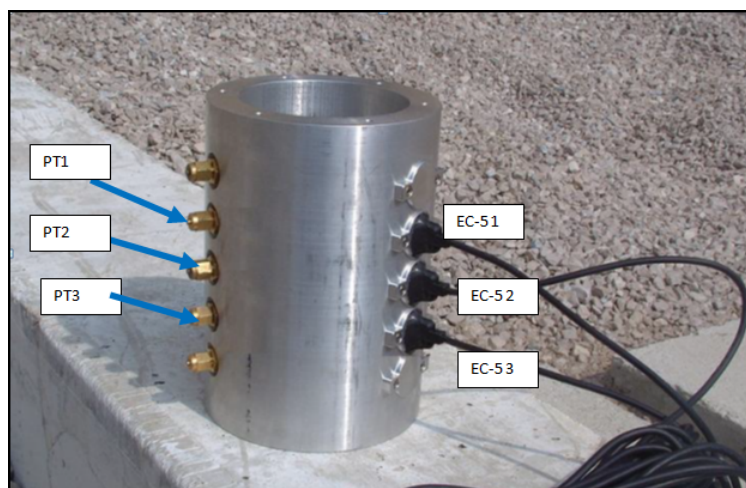
Figure 3.1: Aluminum pressure cell. The pressure transducers (PT1, PT2 and PT3) can be seen on the left. The moisture sensor EC-5s can be seen on the right. Reproduced from [32].

The aluminum chamber has two end caps. A fine mesh grid is placed at the outlet cap to prevent the soil particles from obstructing the opening.

3.2.2   Wetting Phase Tensiometers and Pressure Transducers

The pressure of the water (the wetting fluid) is measured with tensiometers (shown in Figure 3.3). It consists of a hydrophilic porous ceramic cup that is 2.86 cm long and 0.64 cm outer diameter (0652 x 03-B1M3, Soil Moisture Corp., Santa Barbara, CA, USA [32]). It is connected through a Swagelok fitting to pressure transducers (FP2000, Honeywell, Columbus, OH. USA) [32] [60]. The pressure transducers are connected to a data-logger (CR7, Campbell Scientific, Logan, Utah). The calibration of the pressure transducer is reported in Appendix A.

3.2.3   Soil Moisture Probes: EC-5

The water content (wetting phase) in the media is measured using the soil moisture sensors, EC-5s (by Decagon, WA. USA). They measure the dielectric permittivity of the medium using the capacitance technique [32] [60]. The probes, as shown in Figure 3.2, are vertically oriented along the column to minimize the interference on the vertical water flow [32]. To minimize interferences of the aluminum chamber, the EC-5s are calibrated

inside the column with the two-point method developed by Sakaki [61] and previously successfully applied by [32] [58] [59] [60] and [62]. To improve sensor performance, the calibration (described in Appendix A) was repeated before every experiment.

Figure 3.2: Tensiometer with porous ceramic cap. Reproduced from [32].

3.3   Methods

3.3.1   Soil Composition

The section describes the methodology adopted to analyze the growth media particle size distribution and soil components. In order to quantify the changes of organic content and fines loss over time, fresh and used green roof media have been tested and compared.

3.3.1.1   Grain size distribution

The grain size distribution was determined through sieve analysis. It is a procedure in which the soil is sieved through several sieves with decreasing mesh sizes. The sieves covered a range from 0 μm (the pan) to 11200 μm (as reported in Table 3.1) and they have been classified into three categories:

- Fines: this category includes the pan up to the sieve number 140 (the number represents the size of the mesh, as shown in Table 3.1).
- Medium size: from sieve 100 to 40;
- Coarse: from sieve 20 to sieve 0.375.

Prior to sieving, every soil sample was oven dried (at 65°C for 24 hours). The sieves were then shaken in the tumble machine for 8 minutes.

Table 3.1: Sieves utilized for the analyses and their respective numbers and mesh size or openings

Sieve #	Sieve opening (μm)	Particle Category
0.375	11200	Coarse (d>2000μm)
4	4750	Coarse (d>2000μm)
10	2000	Coarse (d>2000μm)
20	850	Medium (2000μm >d>150μm)
40	425	Medium (2000μm >d>150μm)
60	250	Medium (2000μm >d>150μm)
100	150	Medium (2000μm >d>150μm)
140	106	Fine (150μm >d)
200	75	Fine (150μm >d)
Pan	0	Fine (150μm >d)

3.3.1.2   Mass Loss

To quantify the eventual loss of fine particles when the soil is flushed by water (or rain) a sample of fresh soil was sieved before and after the experiment which consisted of flushing the specimen with D.I. (De-Ionized) water. The volume of water flushed was equal to 30 times the pore volume of the sample (V_V). According to the calculated pore volume, the amount of water required per flushing was 19 liters and this procedure was repeated three times. The outflow was collected into a tank and a water sample was taken prior to flushing for the next test.

3.3.1.3   Organic content

Similar to [39] and [63], the organic fraction (by mass) of the soil was determined by dry combustion. The soil samples were placed in crucibles and transferred in the muffler oven at 550°C for 2 hours. Prior to this process, the soil samples were oven dried (at 65°C for 24 hours) to remove the water content. The difference of weight of each crucible, before and after the combustion, indicates the organic mass lost in combustion. The organic content was measured for the fresh and old media. For the fresh media, 6 soil samples were selected, while for the old soil, each of the nine section was sampled three times.

3.3.2 Saturated Hydraulic Conductivity

The measurement of the saturated hydraulic conductivity (K), even if it is usually a standard procedure, poses several challenges for the green roof growth media. Three different methodologies have been tested. The first one was the procedure used for the apparatus (the pressure cell), as described by [32], the second is the ASTM method for saturated hydraulic conductivity and finally the third, which provided improved results, consists on a modification of the first method.

According to the initial method (applied by [32]), the aluminum soil chamber was filled with dry soil (the bulk density was kept the same in every experiment) and the medium was flushed with 30 pore volumes of DI water. Prior to the experiment, the media was flushed with carbon dioxide for 30 minutes to saturate the pore space with carbon dioxide instead of air. Since, CO_2 is more soluble in water than air, it facilitates the saturation of the media. The outflow from the pressure cell was collected in a beaker placed on a precision scale that recorded the incremental weight in g/sec (equal to cm^3/sec). The volumetric flow (Q) was converted into Darcy's velocity (q) in cm/sec by dividing it by the cross sectional area (A) of the column, in cm^2. Although this method was successful for sand in [32], it posed several problems for the green roof growth media; the water pressure readings of the pressure transducers along the column were often not consistent with the expected results and the results were not repeatable.

The second method that was attempted was the constant head ASTM method head. The method consisted of placing a soil sample into a permeameter with two porous discs (one made of stone and one made of timber) at both ends. The sample was saturated with water and one end (the inlet) is connected to a constant head reservoir of water. The other end (the outlet) is connected to a graduated beaker (the flow direction can be upward or downward). The time at which the outflow reaches a certain volume in the beaker was recorded manually with a stopwatch and the experiment was repeated several times (at least 3) for each head level (the reservoir was placed at different heights to have different head). As before, the method was successfully applied on sand; however, it posed problems with the green roof growth media. With the first method, the main challenge was to record the correct head pressure inside the column. On the other hand, with the

second method, the main problem arose from the heterogeneity of the soil components: after repeated flushing the particles separated into layers according to their weights. This resulted in inconsistencies; the time at which the flow filled a certain volume was not constant, even if the reservoir of water was kept in the same position.

A third approach was attempted, similar to the initial set up, where the medium was placed inside the soil chamber with the same packing procedure. The soil chamber, sealed at both ends, was flushed upward. The inlet was connected to a peristaltic pump and the outlet was flowing into the precision scale. The pressure head was measured at the bottom and at the top of the column with two piezometers (two graduated glass burettes), as shown in Figure 3.4. This last configuration successfully allowed measuring the saturated hydraulic conductivity with repeatable results (the results are discussed in Chapter 4). The method was also tested on sand and gave results consistent with the literature (reported in Appendix B).
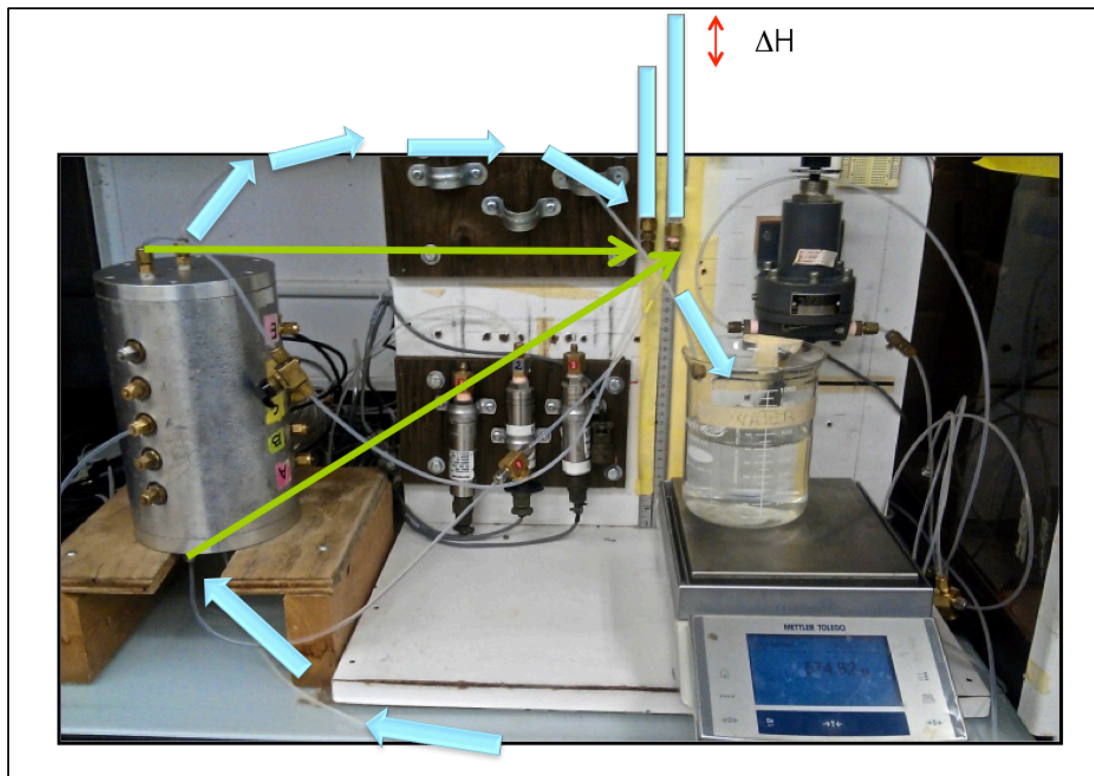
Figure 3.3: Experiment set up of the third method. The blue arrows indicate the water flow, which is injected from the bottom of the column and it comes out from

the top, ending in the beaker on the precision scale. The blue bars on the right represent the two piezometer-burettes that show the water pressure at the bottom and at the top of the soil chamber (the locations are pointed by the green arrows) and ΔH represents the difference of head. The full length of the piezometers is not included in the picture, which provide a simplified illustration.

Since the water pressure reached higher values than the burettes' length, the set up was modified by replacing the two burettes with other longer ones (2 m long), that were installed on a vertical panel.

The incorrect hydraulic conductivity results of the other two methods are reported in Appendix C.

3.3.3   Water Retention Curve ($P_C - S_W$ Relationship)

To investigate the $P_C - S_W$ relationship of the growth media, the apparatus described in the previous section was utilized. The method was successfully applied in [64] [59] [65] [65] for studying the dynamic capillarity effects in sand.

The EC-5s, connected to the data-logger CR7 (Campbell Scientific) provided readings in mV, which can be converted into volumetric water content (θ) (the method is described in Appendix A). Then, the water saturation can be calculated [15] as follows:

$$Sw = \frac{\theta}{\phi} \qquad\qquad 3.1$$

where ϕ is the porosity of the soil and can be calculated [15] as follows:

$$\phi = \frac{V_V}{V_T} \qquad\qquad 3.2$$

or

$$\phi = 1 - \frac{\rho_b}{\rho_S} \qquad\qquad 3.3$$

The bulk density (ρb) was always maintained close to the same values (1.03 g/cm^3) in every experiment. This value was reported in the laboratory analyses conducted on the same green roof media by [66] at the instance of [3]. During the packing, the soil is placed one layer (2 cm thick) per time in the soil chamber that is shaken to evenly distribute the soil particles. The volume of voids (V_V) is calculated [15] as follows:

$$V_V = V_T - V_S \qquad\qquad 3.4$$

where V_S is the volume occupied by solids and is calculated as follows:

$$V_S = \frac{M_S}{\rho_S} \qquad\qquad 3.5$$

The particle density (ρ_S) is usually estimated from the soil composition; however, it was necessary to measure it for the green roof soil. The particle density was measured with a simple procedure: a known volume of water (V_1) was poured into a graduated cylinder and then a known amount of growth media (M_{dry}) was added. The consequent volume rise (up to V_2) indicates the volume that the soil particles occupy in the graduated cylinder. Therefore, the volume of solids (V_S) can be obtained as the difference between V_1 and V_2. The solid density can then be calculated as $\rho_S = M_{dry}/V_S$.

The water pressure was measured with the pressure transducers, from which the readings in mV can be converted in centimeters of water with the calibration coefficients (the calibration is described in Appendix A). The readings of the pressure transducers refer to the water pressure inside the column and, as previously described, the capillary pressure (P_C) can be calculated as the difference between the pressure of the air and the water. Since the top of the column is open to the atmosphere, the pressure of air (P_{NW}) can be assumed to be zero, therefore P_C is equal to the water pressure with the opposite sign.

When the wetting curve starts with dry soil, the curve is usually called the *primary imbibition* curve; it represents one of the two boundary curves of the $P_C - S_W$ relationship. Dry soil provides the opportunity to study the $P_C - S_W$ at extremely low saturation level, from $S_W = 0$ to full saturation, which otherwise would not be possible. Once the column is packed with dry soil, D.I. water is then slowly injected from the

bottom of the soil chamber till the water reaches the edge of the column. During the wetting process, the EC-5s and pressure transducers record the water content and water pressure. During the drainage test, the valve, connected to the outlet at the bottom of the pressure cell, is partially open and the water drains slowly.

In one experiment, to enhance the water loss though evaporation, the soil chamber was heated with a heating plate. After the water drained due to gravity forces, the heating plate was turned on. The heating was applied with intermittence: when the soil temperature reached 30-40°C at the surface, the plate was turned off to let the soil cool down. During the heating and the cooling periods the measurements have not been taken in consideration, since the EC-5s are sensitive to high temperatures.

3.3.4   Thermal Properties

3.3.4.1   Laboratory Measurements

As mentioned in Chapter 2, the thermal properties can be measured with different methodologies and the method adopted in this study employed a commercial device, the thermal properties analyzer KD2 Pro, by Decagon. It consists of the two-needle SH-1 probe (as shown in Figure 3.5) and each needle is 30 mm long with a diameter of 1.3 mm and having 6 mm spacing between the two needles). It is also utilized by [7] [12] [62].

Figure 3.4: Two-needle probe SH-1 of the thermal properties analyzer KD2 Pro by Decagon (reproduced from [67]).

The device system is based on a transient line heat source method [67], also described in IEE 442-1981 and ASTM D5334, as reported by [12]. The device is able to simultaneously measure 4 thermal properties (thermal conductivity, diffusivity, resistivity and volumetric heat capacity). The probe generates a heat pulse into the surrounding medium and both needles measure the temperature rise over time [7]. The KD2 Pro takes a set of measurements (taken at one second interval) over a period of 30 seconds of heating and 30 seconds of cooling. The sensor has an uncertainty of 5%; however, according to the authors in [7] and [12], who tested different green roof media, the soil variability increases the uncertainty to 10%.

As mentioned in Chapter 2, measuring only the thermal properties of the media is not sufficient to characterize the soil behavior because these properties are affected by several soil characteristics such as the water and organic content. Therefore, in the study, the thermal properties are analyzed under different condition of soil moisture content. The methodologies adopted are two: *beaker method* and soil *chamber method*.

In the beaker method, three samples of growth media, with a volume of 500 cm^3 each, were placed into a cylindrical glass container (the bulk density was maintained close to 1.03 g/cm^3). The thermal properties were analyzed three times per sample using the KD2 Pro probe. The moisture content of each soil sample was gradually increased (20 mL of D.I. per time). To assure an even moisture distribution, each sample was placed into a flat pan and it was homogeneously mixed with the water and replaced in the container. This methodology was initially tested on sand and the results were consistent with values reported by [62], where the same thermal properties analyzer KD2 Pro was utilized (the results are reported in Appendix B).

With the second method (chamber method), the thermal properties were measured directly inside the soil chamber during the drainage experiment. The probe SH-1 was inserted horizontally in the medium at the same level of the first EC-5 (as shown in Figure 3.6) and it was programmed to take measurements automatically (every 15 minutes). At the same time, the moisture sensor continuously measured the moisture

content (every 1 minute). This methodology allowed taking a greater number of measurements over time.
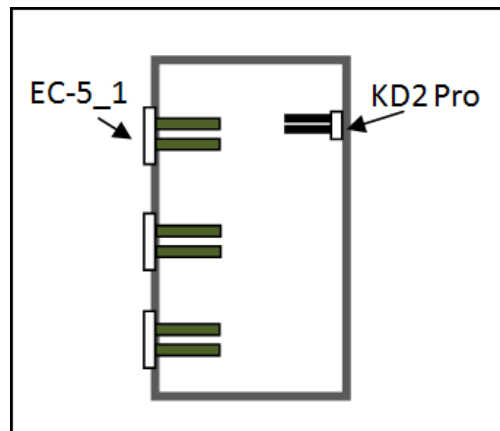
Figure 3.5: Scheme of the soil chamber with the three EC-5s (on the left) and the KD2 Pro (SH-i Probe) inserted horizontally (on the right). EC-5_1 is at the same level of the SH-1 probe.

3.3.5   Testing Used Green Roof Media

To test the used soil, one module was taken from the green roof in London (the roof is approximately 2.5 years old). During a previous study, conducted by [63], the module was divided into 9 sections: the surface was divided into three rows (as shown in Figure 4.5) and each of them was divided in three layers along the depth of the module; the layer number 1 is the closest to the surface.
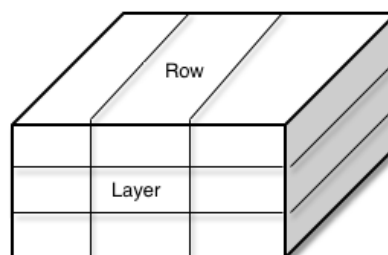
Figure 3.6: Partition of the green roof module into rows and layers.

Before measuring the thermal properties the soil samples were first oven dried (at 65°C for 24 hours), cooled down at room temperature and placed in containers (glass beakers of 500 mL volume) with the same bulk density (ρ_b = 1.03 g/cm^3).

3.3.5.1   Field Measurements

With the same device (KD2 Pro) the thermal properties have also been measured in the field, at the green roof site on Talbot College (Western University, London, ON). The measurements have been taken on three different modules of the green roof (as it is further explained in Chapter 4); one module was vegetated with *Aquilegia*, one with *Grass* and the last was bare soil. The measurements have bee conducted every morning (from 8:00 to 9:00) from June 17 till June 26 (2013). On each module, the KD2 Pro was inserted perpendicular to the soil surface and the measurements were taken into five different locations and the average among the five measurements was taken.

Chapter 4 - Results

4   Introduction

In this chapter the results of the growth media characterization for *fresh* and *old* soil are reported. As discussed in Chapter 3, the term *fresh soil* refers to the growth media that have never been used on the roof, while *old/used soil* refers to the media sampled from the green roof in London (ON).

The results are grouped into three main categories, based on the type of properties that are measured:

- Soil composition: in this section the grain size, soil composition and organic content of the fresh and used soil are reported.
- Hydraulic properties: saturated hydraulic conductivity and the $P_C - S_W$ relationship under different conditions are discussed.
- Thermal properties: thermal properties of the fresh and old green roof soil in relation to water content are reported. This section also includes the field measurements at the green roof on Talbot College at Western University campus.

4.1   Soil Composition

4.1.1   Particle Size Distribution

To analyze the particle size distribution, three samples (600g each) of fresh soil are tested. The results are reported in Figure 4.1. The Figure also reports the sieve analysis on used soil that will be further discussed in the section.
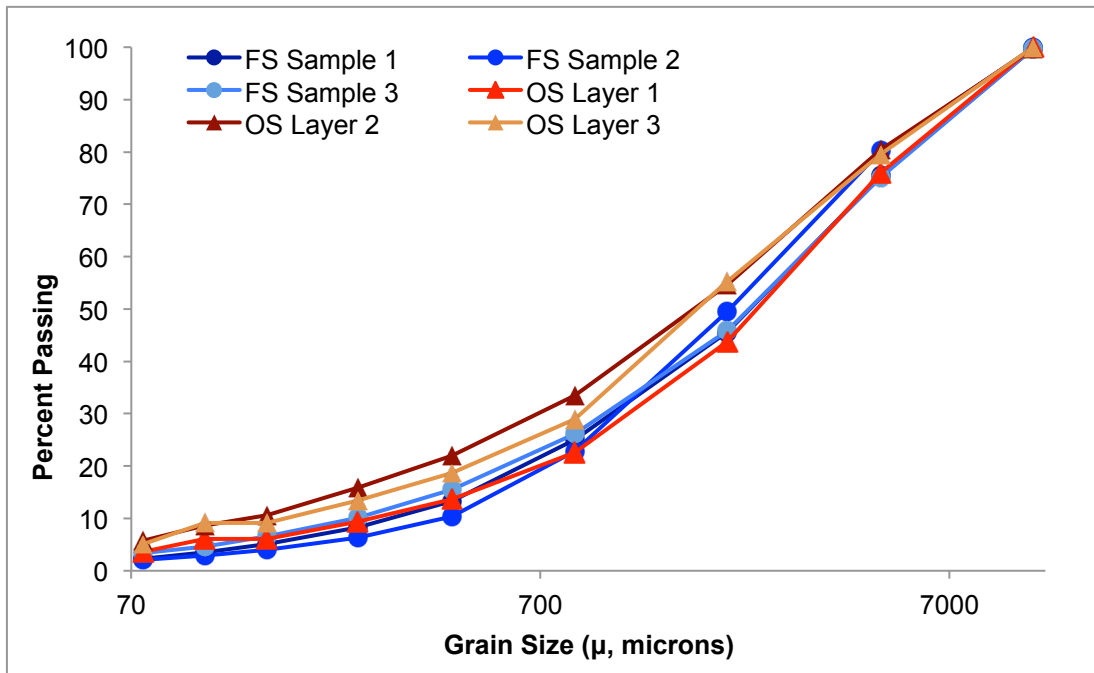
Figure 4.1: Sieve analysis of fresh soil (FS) and old soil (OS). Each FS curve represents one soil sample while each OS curve represents one layer of the green roof module.

 All the three samples presented a heterogeneous grain size distribution. The average uniformity index (UI) for the three samples is UI= 15, where the large-size particles have a diameter d>150μm and the small-size particles consist of the remaining fraction (i.e. the fines). Approximately 50% (by mass) of the soil consists of *coarse material* (d>2000μm); the remaining fractions consist of *medium* size particles (around 40%, 2000μm<d<150μm) and *fine* particles (around 10%, d<150μm). According to the FLL guidelines [17], the content of fine particles of silt and clay with d<64 mm should not exceed 15% by mass of the substrate for extensive green roofs; therefore the growth

media here analyzed respect the limit. The fine fraction (shown in Figure 4.2) represented several challenges for the soil characterization. For instance, as shown in Figure 4.3, the material presents a strong hydrophobic behaviour when dry; therefore, reaching full saturation conditions was often difficult during the hydraulic conductivity and the P_C-S_W tests and to measure thermal properties and the water content for saturated soils. Moreover, this initial high hydrophobic characteristic strongly affects the hysteresis of the P_C-S_W relationship. Indeed, to high hysteresis corresponds a low soil wettability [68].

Figure 4.2: Fine components of fresh green roof soil. The jar in the left contains the particles smaller than 75 µm. The jar in the middle contains the particles retained by the 75-µm mesh. The jar in the right contains the particles retained by the 106-µm mesh.

Figure 4.3: The fine material (with grains smaller than 75 µm) presents a hydrophobic behavior when dry. The picture shows some droplets of water on the surface of the fines.

As a further investigation, the sieve analysis was also conducted on components of the growth media (Figure 4.4). The components chosen are the fine and coarse expanded shale (which represents the major volumetric fraction of the growth media) and the limestone. LiveRoof provided the expanded shale (fine and coarse). In terms of fines, the fine-expanded shale presented 5.11% by mass, while the limestone had the highest percentage of fines, approximately 17% by mass. This test helped to better understand the soil composition; moreover, it can be concluded that most of the fine fraction consists of limestone, the heaviest component of the growth media. As will be further discussed, this fact can enhance the fines loss in the green roof because heavier fine particles are more easily flushed away over time.
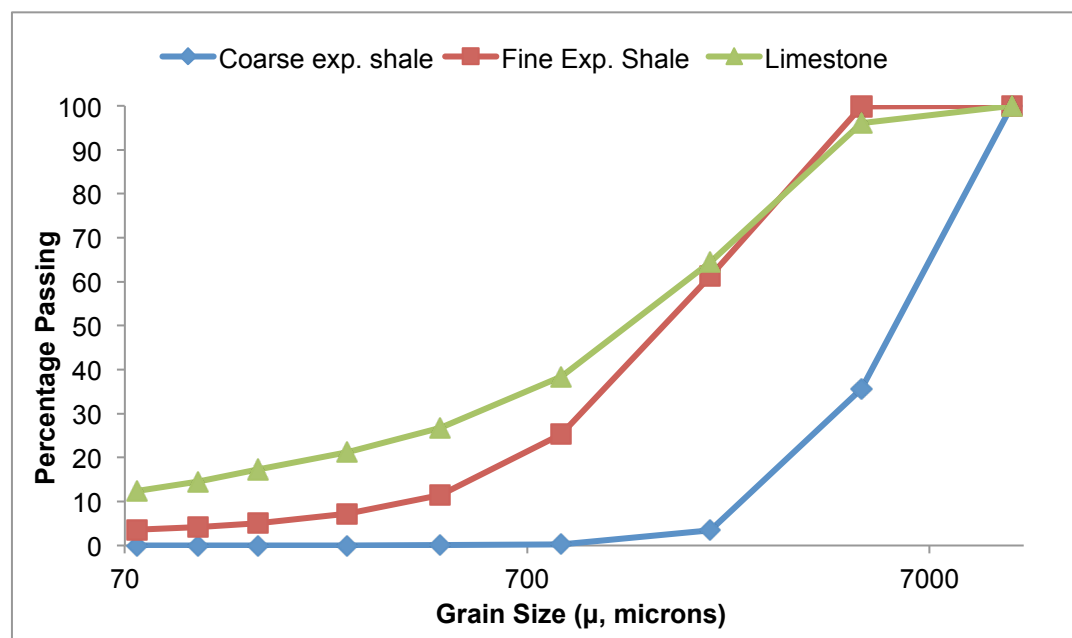
Figure 4.4: Sieve analysis of coarse and fine lightweight material (expanded shale) and limestone.

A third test was performed on used growth media to assess the extent to which weathering and interaction with plants could impact composition with time. As described in Chapter 3, the used soil consists of one green roof module taken from the green roof site at Western University. The module was divided into 9 sections listed in Table 4.1. The surface of the module was divided into three rows and each row was divided into

three layers along the entire depth of the module. The surface layer is referred as L1, the middle layer is L2 and the bottom layer is L3. The sieve analysis was conducted per each section and Figure 4.5 shows the average of the three rows.

Table 4.1: Partition of the green roof module into Layers and Rows, for a total of nine soil samples.

Layer X Row	Row #1	Row #2	Row #3
Layer #1 (top)	R1L1	R2L1	R3L1
Layer #2 (middle)	R1L2	R2L2	R3L2
Layer #3 (bottom)	R1L3	R2L3	R3L3

According to the results, fresh and old soil presented similar grain size distributions (as shown in Figure 4.1), however, it was noticed that the percentage (by mass) of fines in the used media was lower than the percentage in the fresh one, as shown in Figure 4.5. The percentage of fines increases with the depth of the module: Layer 1 has the lowest content while Layer 3 the highest. This can be explained by the fact that the rainwater, which flows through the media, flushes the fines away from the surface to the bottom and some of the material is lost over time.
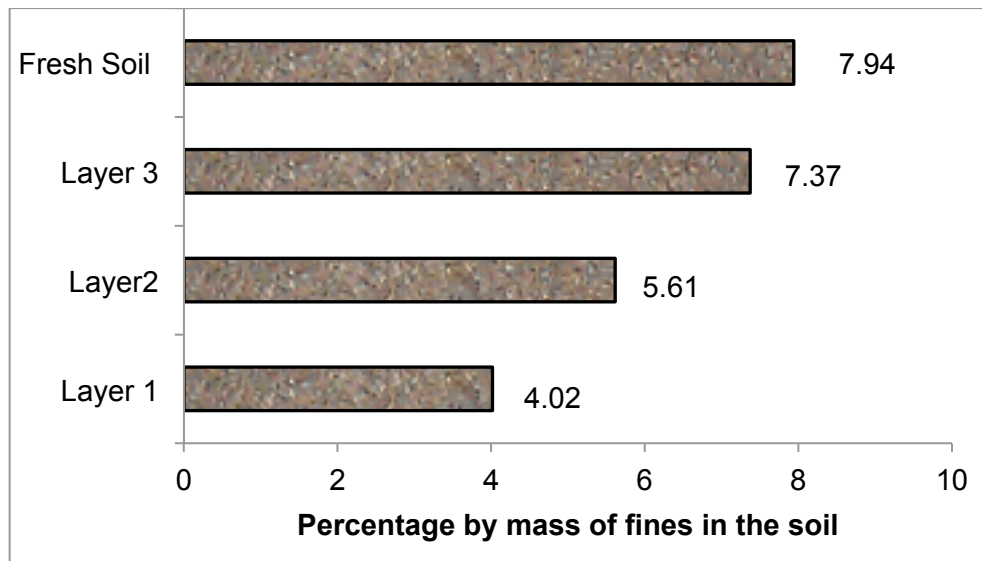
Figure 4.5: Comparison of the fines percentage (by mass) between fresh and old soil.

In order to quantify the amount of fines that the soil can lose when exposed to the rainfall events, the sieve analysis was conducted on a sample of fresh soil (also never used in laboratory) before and after flushing for three times a volume of water equal to thirty times the pore volume. The total volume flushed was 2419 mm.

Figure 4.6: Water collected in the tank after that the column was flushed with 19 liters. Deposition of fines can be observed at the bottom of the tank.

The water samples were analyzed with a nephelometer to measure the turbidity (in NTU, Nephelometric Turbidity Units). As reported in Table 4.2, the turbidity notably decreases with the amount of water flushed through the media.

Table 4.2: Turbidity analysis. As the NTU increases, the turbidity of the water sample also increases.

First flushing (2419 mm)	18.13 NTU
Second flushing (2419 mm)	10.01 NTU
Third flushing (2419 mm)	3.15 NTU

After the soil was flushed, it was dried in the oven and sieved again. 2419 mm is more than the double of the yearly precipitation in London (Ontario) [69], however, the difference in the percentage of fines before and after the flushing was approximately 1% by mass compared to 4% on the green roof (regarding the upper layer). Given this flushing protocol is not adequately representative of fines loss observed on the used green roof (and reported in Figure 4.5). This could be because of differences between the outlets of the soil chamber and the green roof module. In the soil chamber there is one 5 mm diameter outlet while the green roof module provided by LiveRoof presents more and larger apertures, as shown in Figure 4.7.
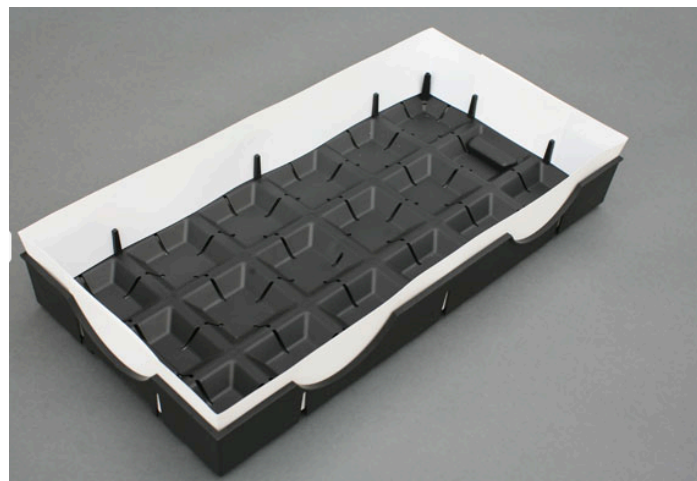
Figure 4.7: Empty module for the green roof (reproduced from [3]).

4.1.2   Organic Content

The organic content of the growth media was determined by dry combustion. The averaged organic content of the three rows per each layer for the fresh and old soil are reported in Figure 4.8. From the results, it appears that L2 and the fresh soil have similar organic content. The lowest layer (L3) has the lowest organic content while L1 presents the highest.
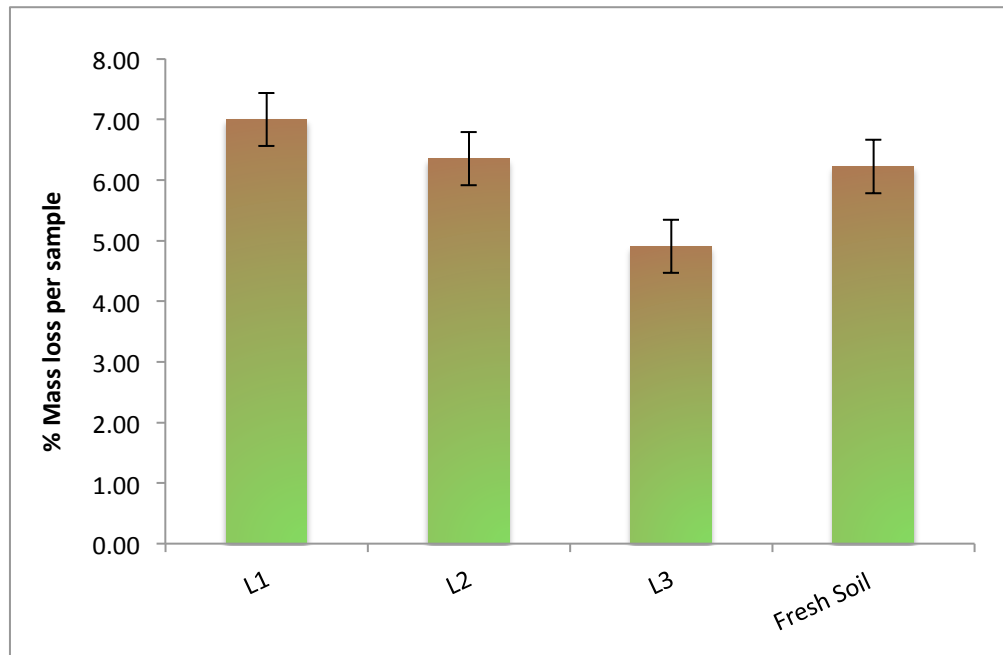
Figure 4.8:Percentage of organic content of each layer. The last bar represents the fresh growth media. L1, L2 and L3 refer to the layer, where L1 is the closest to the surface. The error bars represent the 95% confidence interval of the mean.

The higher organic content in the upper layer (L1) is due to the presence of plants. Indeed, despite the plants and the roots have been removed from the module before the laboratory testing, the plants naturally lose leaves and organic materials, which over time sediment on the surface layer (L1). On the other hand, the lowest organic content in bottom layer (L3) is because the plants utilize the organic matter up taking nutrients from the roots.

4.2   Hydraulic Properties

4.2.1   Saturated Hydraulic Conductivity

The saturated hydraulic conductivity of fresh growth media was tested with the third method, as described in Chapter 3. The experiment has been conducted three times and the results are reported in the following Table 4.2 and illustrated in Figure 4.9. The hydraulic gradient ($\Delta H/\Delta L$) is on the horizontal axis and the Darcy's velocity (q) is on the vertical axis. As described in Chapter 3, according to the Darcy's law (eq. 2.1) the slope of the plot represents the saturated hydraulic conductivity (K, cm/sec).

Table 4.3: Saturated hydraulic conductivity for three experiments.

	Trial 1	Trial 2	Trial 3
K (cm/sec)	0.0166	0.0168	0.0166
R^2	0.978	0.987	0.991
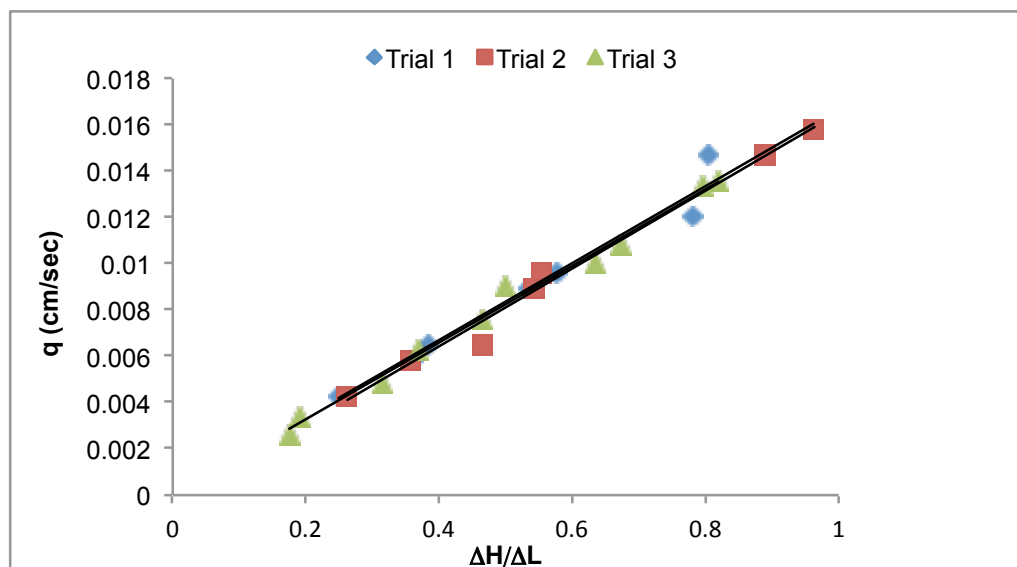
Figure 4.9: Saturated hydraulic conductivity (the slope) of the green roof media. Trial 1, 2 and 3 represent three tests. In the chart are reported the straight lines of each experiment.

As discussed in Chapter 2, according to the FLL guideline [17], the saturated hydraulic conductivity for an extensive green roof should be higher than 0.0010 cm/sec. According to the analyses made by [66] on the same growth media, K was calculated to be 0.0160 cm/sec. The average value experimentally measured in the thesis (0.0177 cm/sec) meets the FLL standards and it is comparable with the range given by [66]. In comparison with the values reported in Table 2.1, the measured hydraulic conductivity is lower than the conductivity measured for substrates with less or no organic content such as the substrates in [18] [19] [22] [21], and the laboratory blended substrates in [13] [20]. On the other hand, the soils reported in [20] [23] [25], that consist of a mixture of lightweight aggregate (e.g., pumice and expanded clay) and organic matter (compost and composted bark), had measured hydraulic conductivity on the same order of magnitude.

4.2.2   Soil Water Retention Curve ($P_C - S_W$ Relationship)

Several imbibition and drainage $P_C - S_W$ experiments were conducted. It is usually easier to start with the primary drainage curve [16], however, in order to investigate the $P_C - S_W$ curves at low water saturation, it is also necessary to start with primary imbibition. As described in Chapter 3, the water content and the water pressure are measured in three locations along the soil chamber. In the results here reported, the $P_C - S_W$ curves are presented as the average between these measurements at the three locations.

4.2.2.1 $P_C - S_W$ for Fresh Growth Media

4.2.2.1.1   Drainage Curves

Figure 4.10 shows the three drainage curves for the fresh media, each curve is the resulting average of the measurements at the three locations. The first test (Trial 1) was primary drainage. As mentioned in Chapter 2, the term *primary drainage* refers to the drainage that occurred in the soil sample on the first drainage. After this test, the soil chamber is saturated and drained two other times and the drainage curves are respectively named Trial 2 and Trial 3. The packing was the same for each test. Every drainage test took approximately 12 hours and it consisted only of drainage due to gravity (which occurs in the first three hours of the test) and partial evaporation. The black line in Figure

4.10 represents the fitted curve with the Van Genuchten model (the fitted parameters, α and n, are reported in Table 4.4) based on the average of the three drainage curves. As it can be noted in the chart, the three curves start from a water saturation slightly lower than $S_W = 1.0$; this is because during the beginning of the drainage there was always some noise, therefore those data have not been considered.
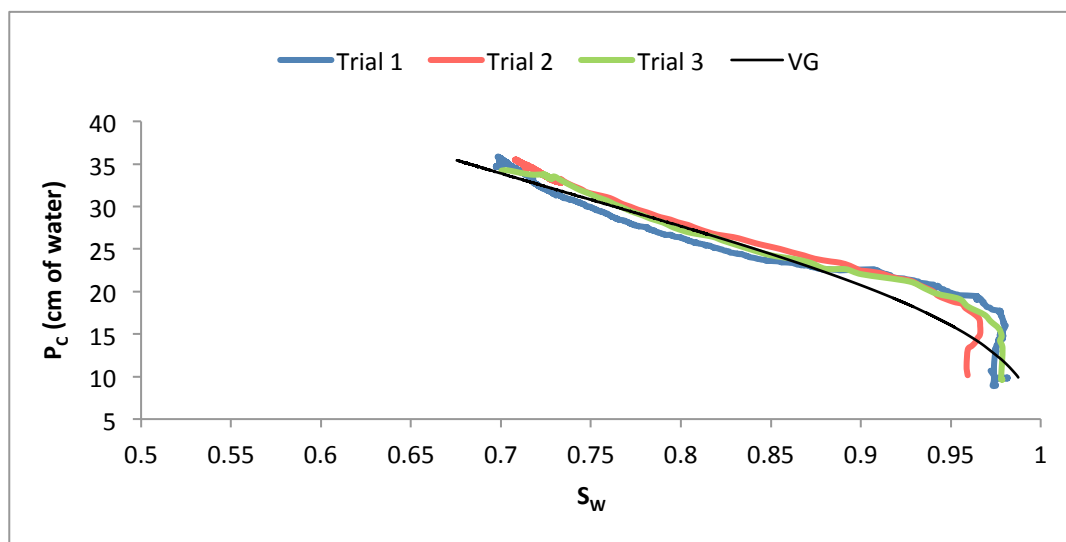
Figure 4.10: Drainage curves due to gravity and partial evaporation. The chart shows three drainage tests (Trial 1, Trial 2 and Trial 3). Each curve represents the average of the curve measured at each location along the column (top, middle and bottom).

As shown in Figure 4.10, there is little difference between the primary drainage curve and the other two curves. The minimum water saturation (S_W) reached during the three drainage tests is approximately 0.68-0.7 with a capillary pressure (P_C) equal to 35 cm of water. From these results it can be deducted that the $S_W = 0.7$ represents the field capacity of the bare soil. The entry pressure can be estimated to be between 15 and 20 cm of water. The amount of water drained from the soil chamber suggests that the soil retains approximately ¾ of the total water following gravity drainage. It was also observed that the soil is able to absorb part of the injected water; therefore, the water that the soil can hold is higher than the calculated total pore volume. The pore volume was calculated for every test as described in Chapter 3. This characteristic was noted during one test in

which the soil chamber was packed only with expanded shale (fine and coarse). The total amount of water injected in the media to saturate the sample was 800 mL, while the calculated volume of voids was 515.5 cm^3; therefore, the water absorbed by the media was approximately 284.5 cm^3. The same phenomenon was also observed during other experiments with fresh soil, during which the total water injected was greater than the pore volume. Regarding the drainage with the expanded shale, the water retained against the gravity pull by the fresh soil was approximately 79% of the total water injected, therefore it is possible to assess that the material, which represents the main component of the green roof media, has a strong water holding capacity.

The field capacity measured in the laboratory is comparable with the data from the field. Fig. 4.11 shows the moisture content measured over the year 2013 at the three green roof locations: London (at Western University), Calgary and Halifax. First of all, it is necessary to specify that the water saturation levels (S_W) reported in the chart are approximate values. Indeed, the mV readings of the three EC-5s installed on vegetated (with *sedum*) modules have been converted into water content with the Sakaki two-point method. However, for these probes the extreme values for dry and saturated soil required for the calibration are not known; therefore, the calibration was applied using the average for the values for the calibration of seven different probes tested in the laboratory (Min=315 mV, Max=630 mV). As shown in the chart, the water saturation levels never exceed 0.8 and the peaks are usually up to S_W=0.7-0.75. Therefore, this information support the laboratory experiments and the field capacity can be reasonably assumed to correspond to this value. From the figure it can also be observed that Calgary is on average drier and this can be more likely due to climatic condition rather than the calibration of the probe, because the probes used the three locations are the same type and provided from the same company. The winter months have not been considered, since the snow and the frozen water affect the moisture readings.
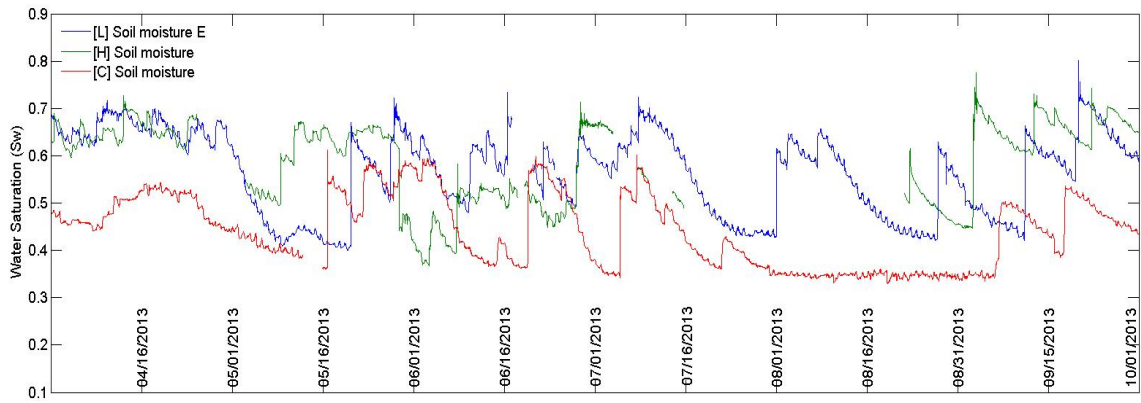
Figure 4.11: Water content measured in London (blue line), Halifax (green line) and Calgary (red line) for the year 2013.

To further investigate the drainage curves at lower saturation levels, other experiments have been conducted. Figure 4.12 summarizes the results for four different drainage experiments, each with a different packing of the soil chamber. The red curve represents the average between the three drainage tests prior discussed (Figure 4.10, noted as the grey dashed line). As earlier mentioned, the drainage occurred mostly for gravity forces; therefore to further reduce water saturation, heat was applied to the base of the column according to the method discussed in Chapter 3. The blue line represents the resulting drainage curve. With the heating plate a lower saturation was achieved (approximately 0.45) with a higher capillary pressure (approximately one meter of water pressure). The experiment was stopped because air bubbles formed inside the tubing at the high temperatures. The green and purple curves (Drainage IV and Drainage V) represent the saturation reduction due to evaporation (following the drainage), which lasted for several weeks. The difference between the curves can be explained because the experiments are conducted on different soil samples with different packing. Therefore, every time the soil is repacked in the soil chamber, the particle arrangement changes, resulting in different configurations of pore spaces. For each experiment the average bulk density was kept constant, however, the porosity calculated was 0.45 for Drainage IV and 0.41 for Drainage V. This last drainage curve (the purple line), reached a very low saturation level (0.05) and a very high capillary pressure (approximately two meters of water). Figure Top also shows the drainage curves modeled with Van Genuchten for each drainage test

(noted by dotted lines). Vulcaflor, Lapillus and Substrate 1 and 2 represent the water retention curves presented in two other studies that will be further discussed in the section.
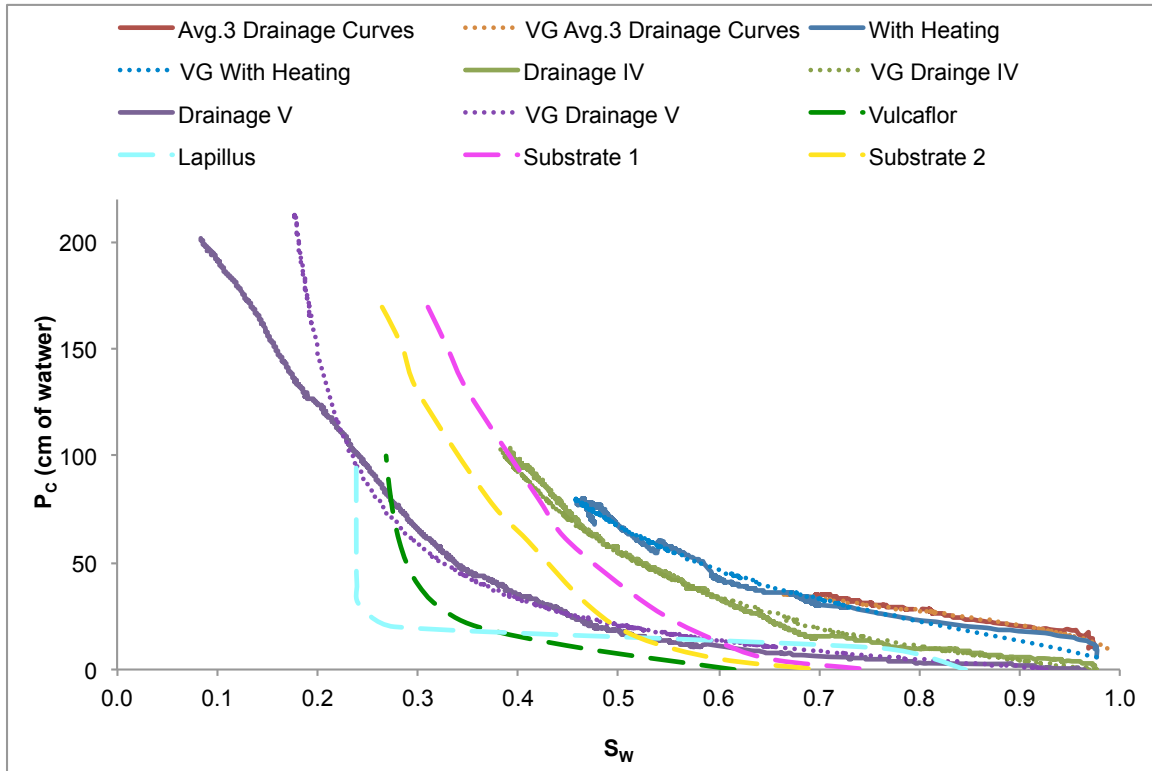
Figure 4.12: Four drainage curves with their modeled Van Genuchten curve (dotted line) noted with the initial "VG". The red line represents the average between the three drainage tests reported in Figure 4.10. The blue line represents the drainage enhanced by heating. The green and purple curves represent a long drainage due to gravity and natural evaporation. The dashed lines represent the drainage curves reproduced from other two studies on different green roof media ([18] [23]).

The parameters of the Van Genuchten model (α and n) have been fitted minimizing the RMSE, which is calculated as follows:

$$RMSE = \sqrt{\frac{(Estimated\ Sw - Measured\ Sw)^2}{n}}$$

4.1

Where *n* is the number of the measurements of the drainage test. The following Table 4.4 reports the fitted parameters per each test and the calculated RMSE.

Table 4.4: Fitted parameter for the Van Genuchten model for four different drainage tests, soil porosity and RMSE.

	Average drainage curves of 3 drainage tests (same packing)	Drainage enhanced with heating	Long Drainage (Trial IV)	Long Drainage (Trial V)
α (cm^{-1})	0.028	0.039	0.039	0.08
n	3	1.8	1.08	1.3
ϕ	0.45	0.41	0.45	0.4
RMSE	0.0084	0.0135	0.0346	0.0616

It should be noted that the VG (Van Genuchten) model is not supposed to describe a water loss that occurred due to evaporation. Indeed, the model describes the drainage, which is a process that occurs due to gravity forces. Therefore, the parameters α and *n* obtained by fitting the drier part of the curve (after the drainage) should be carefully considered because, if applied for other studies, they could not correctly represents the green roof media SWRC.

As mentioned in Chapter 2, in the literature many values of the VG parameters are available for the major textural groups of soils. The authors in [70] [71] cite the table of values proposed by Carsel and Parrish [72]: according to the table, the values of the parameters α and *n* fitted for the green roof soil can be compared with the value corresponding to loam and sandy loam soils, which, as state in the previous chapter, are the most similar to green roof growth media regarding the hydrological behavior.

In the literature, there are not many studies that present measured soil water retention curves for green roof substrates. In the study reported by [18,23] the water retention curves are modeled with Van Genuchten for two green roof substrates, Vulcaflor and

Lapillus, which are based on volcanic materials (pumice, zeolite and lapillus). The parameters θ_r and θ_s have been calibrated on eight storm events, while the parameters α and n have been selected from the table proposed by Carsel and Parrish [72]. Indeed, the authors approximated the Vulcaflor to loamy sand and Lapillus to coarse sand. The curves are reproduced in Figure 4.12 (green and turquoise dashed lines). Similarly as observed during the P_C-S_W experiments in the thesis, the results reported by the authors show that at low water contents, the capillary pressure presents high values and it drastically decreases as the water content increases. However, the shapes of the curves are considerably different from the measured drainage curves in the thesis. This is because both media have been modeled as loam soils/sand soils. Indeed, as it can be observe from the study reported by [73], based on loam soils, the SRWC present several difference form green roof SWRC. For instance the values of capillary pressure at low water contents were higher (>400 cm of water).

In Fig. 4.12 are also reported two other SWRC curves, which describe two green roof media, named Substrate 1 and Substrate 2. The authors [23] directly measured these SWRC using a tension plate apparatus. The substrates tested have been discussed in Chapter 2 and are summarized here: the first one is made of 70% of compost and 30% of pumice by volume and the second has till gravel instead of pumice. Similarly to the experiments conducted in the thesis, also in this study the water retention curves present a steep increase of the soil suction as the water content decreases. The drainage curves presented a more similar shape to the drainage curves measured on the thesis green roof media. This can be explained that, first of all, the curves have been measured and not modeled with standard soils. Secondly, the substrate composition is more similar to the green roof media of the thesis, high in organic content.

4.2.2.1.2   Imbibition Curves

In this section, the results of primary imbibition tests (i.e. wetting the dry soil for the first time) are reported. In Figure 4.13 three primary imbibition tests are reported and from the figure it can be observed that at the beginning of the test, the soil exerts a strong suction. For example the capillary pressure was 1 m to almost 3 m of water pressure when the soil

was completely dry. Maximum capillary pressures differed because the soil chamber was repacked with new dried soil before every test. As such the soil contacting the ceramic caps that were connected to the pressure transducers differed from experiment to experiment. However, a common behavior is observed: the capillary pressure is high at the beginning of the test and, as the water saturation increases, abruptly drops to low values near to zero (cm of water). Every imbibition test has been conducted injecting from the bottom one drop every two seconds (approximately 0.025 mL/sec).

In addition, from the chart it can be observed that when $S_W \cong 1.0$, the capillary pressure becomes negative. This phenomenon can be explained by the fact that, during the imbibition, at high water saturation levels, the soil slightly expands. This soil expansion may exert positive (compression) pressure on the pore water. As discussed in Chapter 2, the capillary pressure is calculated as the difference between the air pressure (P_a, which is null) and the water pressure (P_w). When the soil is unsaturated, the water pressure is negative ($P_w < 0$) due to the soil suction; therefore, $P_C > 0$. At soil saturation, $P_w = P_a$, therefore $P_C = 0$. If the soil matrix expands, the water pressure may assume positive values ($P_w < 0$) leading to a negative capillary pressure.
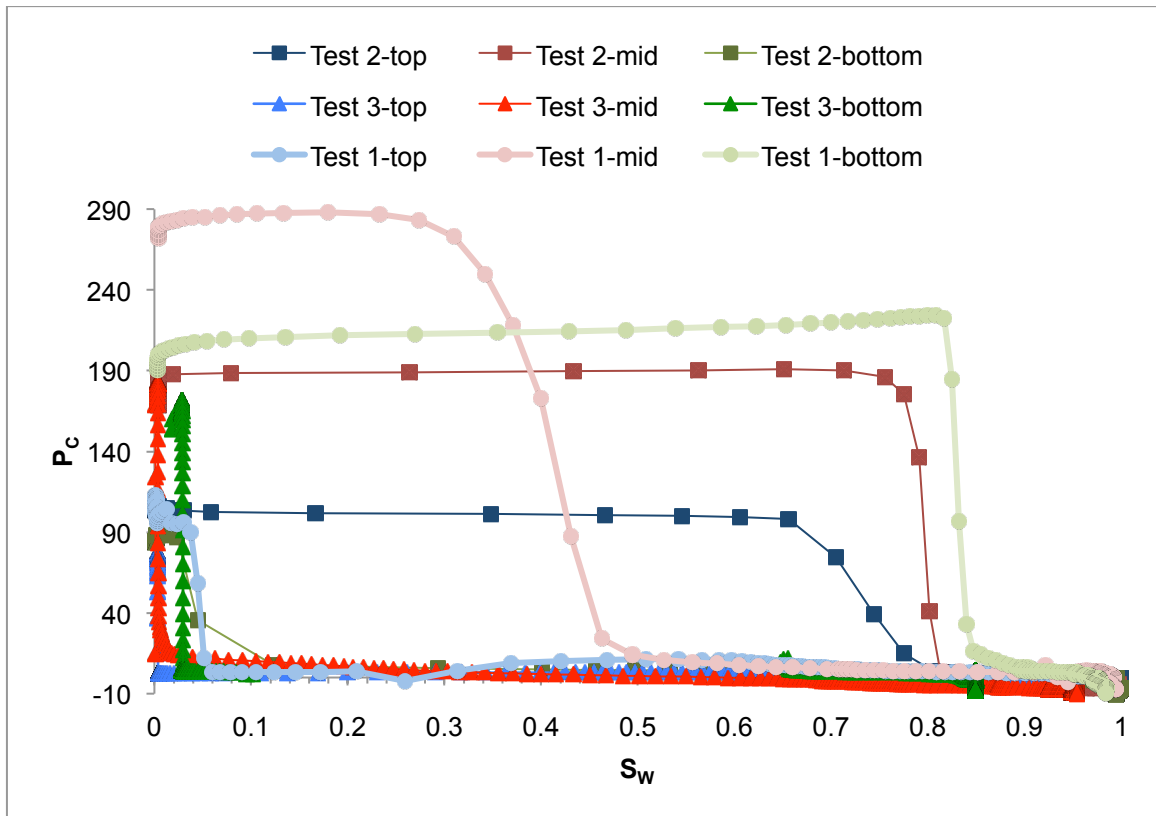
Figure 4.13: Primary imbibition on oven dried soil. The chart shows the primary imbibition of three separate experiments, named as Test1, Test 2 and Test 3 (each experiments consists on a new packing of the pressure cell).

The following Figure 4.14 shows four curves: two imbibition curves and two drainage curves. All four tests have been conducted on the same soil sample in the pressure cell without repacking. The first test (Imb I) consists of a primary imbibition on oven-dried soil. The second test (Drain I), the drainage, followed the primary imbibition. This cycle of imbibition followed by drainage was repeated another time (Imb II, Drain II).

In the primary imbibition test (Imb I), as illustrated in Figure 4.14, the initial capillary pressure started from high pressures and it drastically dropped down close to zero. The second imbibition test (Imb II) started from a saturation level between 0.35 and 0.3 and presented a similar behavior (steep decrease in water pressure). In the chart the modeled Van Genuchten curves are also illustrated (noted by the dotted lines). The model was not applied on the primary imbibition because the experiment started with oven-dried soil.

The fitted parameters are reported in Table 4.5. As shown in the figure, there is a consistent difference between the imbibition and the drainage curves (hysteresis), while the two drainage curves are similar.
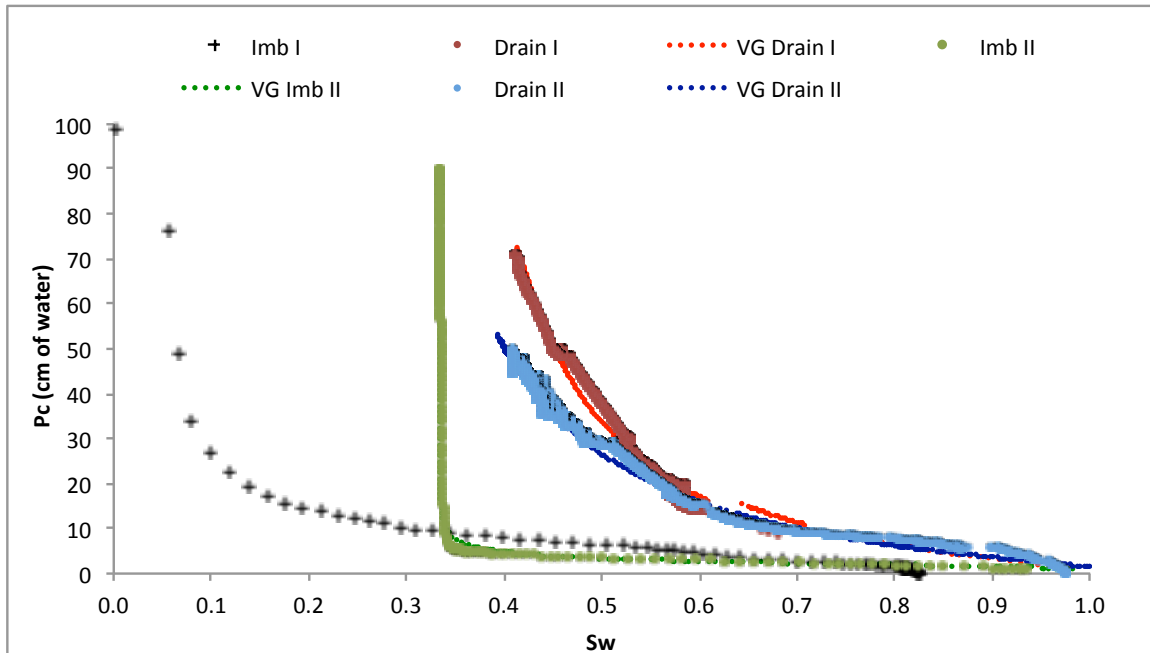
Figure 4.14: Two cycles of imbibition and drainage. The first cycle consists of a primary imbibition (Imb I), followed by drainage (Drain I). The second cycle is the imbibition conducted after the first drainage (Imb II) and the following second drainage (Drain II). In the chart are also reported the curves modeled with Van Genuchten.

The imbibition curves of Figure 4.14 have similar shapes to the imbibition curves of the experiments prior discussed, starting from high values of capillary pressure and presenting a steep decrease as soon as the water content increases. Similarly, the drainage curves presented similar trends and shapes of the prior discussed drainage tests.

Table 4.5: Fitted parameter for the Van Genuchten model, soil porosity and RMSE.

	Drain I	Imb II	Drain II
α (cm^{-1})	0.21	0.036	0.21
n	1.7	4	1.5
ϕ	0.44	0.45	0.45
RMSE	0.0252	0.0153	0.0265

4.2.2.1.3   Effect of the Fine Fraction

To investigate the effect of the *fine* fraction (where *fine* refers to the fraction with particles smaller than 150μm) on the water retention curves, the $P_C - S_W$ experiment was conducted on a soil sample with no fines. The experiment started with a primary imbibition test, followed by drainage and the process was repeated three times on the same packing. The results are reported in Figure 4.15; the imbibition curves are noted with dashed lines, while the drainage curves with round-shaped markers.

As mentioned before, in this experiment it can be noted that the phenomenon of the negative capillary pressure is intensified. This can be explained considering two factors. First, it was observed (during the laboratory experiments of the thesis and during separate experiments conducted in a separate study on the green roof) the expanded shale is the material that exhibits the expansion when moist, so it is reasonable to expect that the soil matrix will exert a higher pressure on the pore water when the soil sample consists mostly of expanded shale. Secondly, since the fine particles that were filling the bigger pore spaces have been now removed, there are less contact points between the grains and the water in between may be more affected by pressure exerted by the coarse grains.
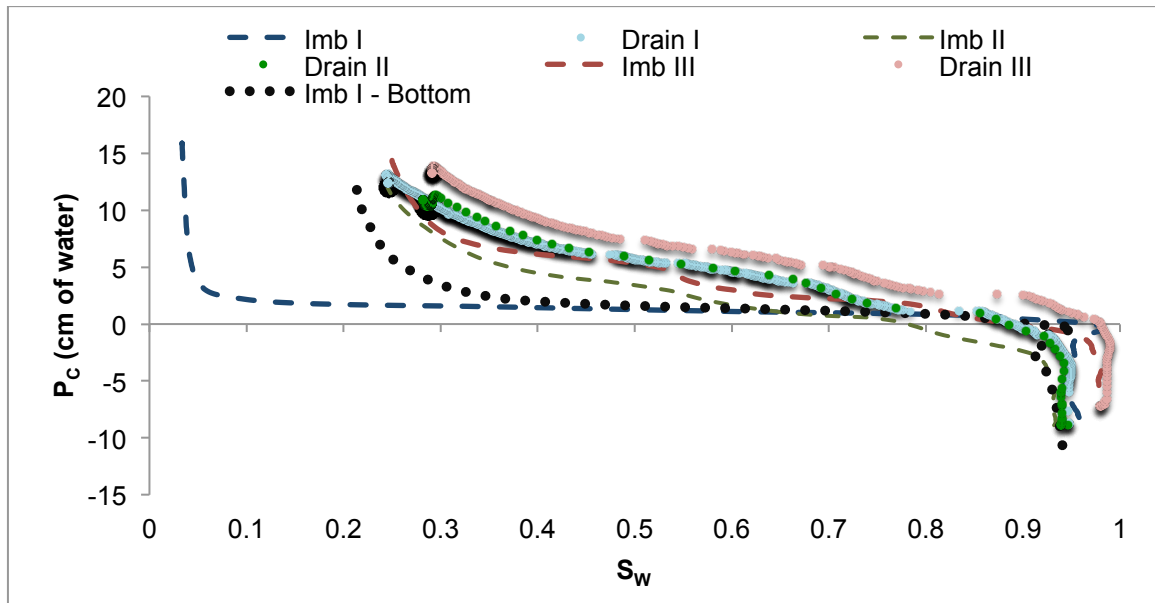
Figure 4.15: Three cycles of imbibition and drainage. The dashed lines represent the imbibition while the solid lines represents the drainage. The numbers (I, II and III) represent the number of the cycle and *Imb I* indicates the primary imbibition. The dotted line represents the primary imbibition occurred at the bottom of the column, where the soil was moist instead of dry.

As before, the curves illustrated in the chart represent the average of the three locations along the column. At the beginning of the primary imbibition, the bottom of the column was slightly moist, therefore, the imbibition curve measured at that location differed from the ones measured in the middle and top locations. This curve is reported in the chart as a black dotted line. It can be observed that all the three drainage curves are similar and that the magnitude of the hysteresis is smaller than for the soil that included fines. This confirms what was stated before regarding the effect of the hydrophobic behavior of the dry fines in relation to the amount of hysteresis. Indeed, the fine fraction, removed from the soil of this experiment, was the component of the media that presented the strong hydrophobicity when dry shown in Figure 4.3.

In comparison with the soil that was not sieved, the capillary pressure during the imbibition and drainage tests are considerably lower. The water drained out due to gravity was almost half of the total water injected therefore the fine fraction has an

important impact on soil water retention. In the field an excessive loss of fine materials over the years can reduce the ability of the green roof to mitigate and delay the peak of runoff. Indeed, according to the results shown in Figure 4.15, the field capacity is much lower, approximately 0.2 of water saturation. As discussed in the previous paragraph regarding the results of the sieve analysis, after one year the growth media has already lost almost 50% (by mass) of the fine material in the surface layer. An observation that can be done is that, as discussed in the paragraph regarding the results of the sieve analysis, most of the fines particles consist of limestone, which is the heaviest component of the medium. Therefore, these heavier particles are more easily washed away from the system.

4.2.2.1.4   Estimation of the Capillary Pressure in the Field

The parameters α and n of the VG model, fitted in the in the laboratory experiments, can be used to estimate the capillary pressure in the field. Because of the reason explained before regarding the accuracy of the parameters for the drier part of the curve (after the drainage), the parameters here selected are the parameters fitted only for the drainage experiments (reported in Table 4.4) . In the following Figure 4.16, the predicted P_C curves for three drainage periods are reported. Water saturation is measured using a EC-5 sensor installed in a vegetated module on the green roof site at Western University. The measurements covered a period from June to July 2014.
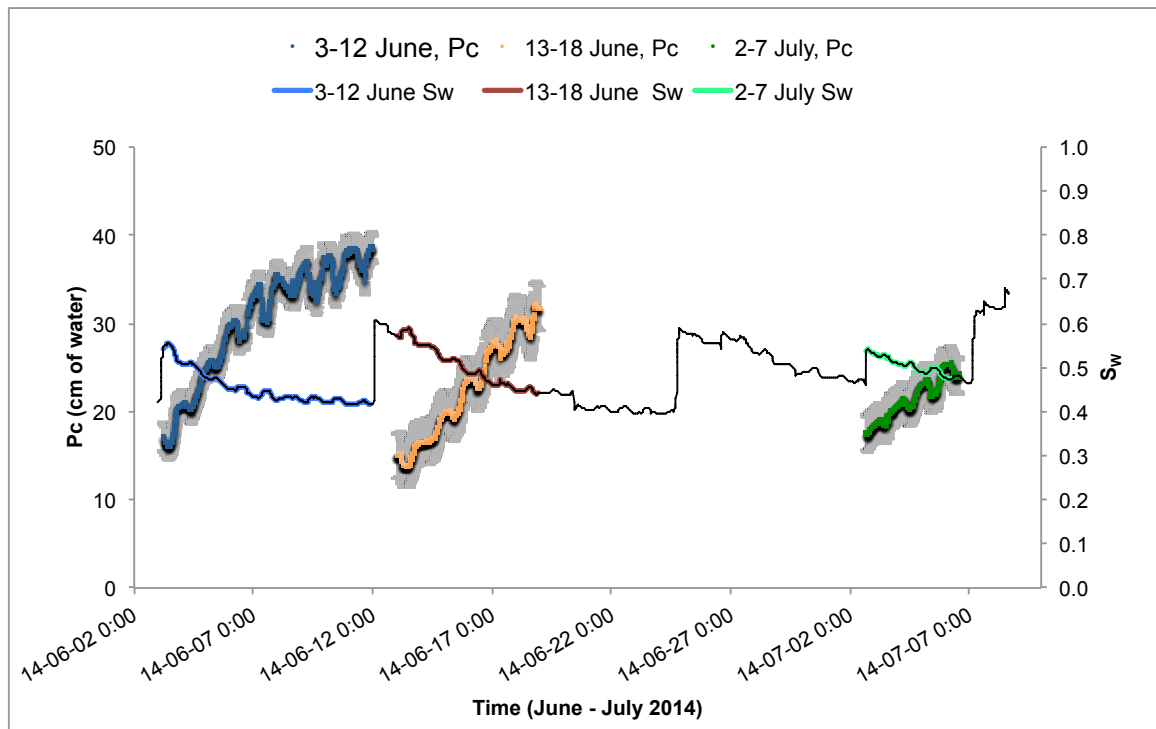
Figure 4.16: Capillary pressure estimated with the Van Genuchten model using the parameters fitted for the secondary drainage reported in Table 4.5. The predicted P_C represents three drainage periods measured on the green roof at Western University between June and July 2014. The grey lines represent the 95% confidence interval of the estimation.

The grey error bars represent the 95% confidence interval regarding the Van Genuchten curve that is based on the drainage test measured in the laboratory and from which are taken the parameters α and n to estimate the capillary pressure of the field data.

4.3   Thermal Properties

In this section the thermal properties measured in the laboratory and in the field are presented and discussed. The first section of the section compares dry fresh and old media tested in the laboratory. The second section presents the thermal properties measured at different water contents in the laboratory and in the field.

4.3.1   Thermal Properties of Old Growth Media (for dry soil)

As described in Chapter 3 the used green roof media consists of media from a green roof module from the London site. The thermal conductivity and the volumetric heat capacity are reported in Figure 4.17 and Figure 4.18. Nine soil samples were tested, one per each section that is defined by row and layer, as listed in Table 4.1. As for the measurements of the organic content, each section was tested three times with the thermal properties analyzer KD2 Pro.

As shown in Figure 4.17, the thermal conductivity increases (statistically) with the depth of the module, with the highest values at the bottom of the module (Layer 3) and the lowest at surface (Layer 1). In comparison with the fresh media, Layer 3 of the old soil had a (statistically) higher thermal conductivity. As previously discussed, Layer 3 has the lowest organic content (Figure 4.8) and the highest fines content (Figure 4.5). On the other hand, Layer 1 has the highest organic content and the lowest fines content. This is in agreement with the literature discussed in Chapter 2, where it was reported that higher organic contents reduce thermal conductivity and an increase of the fine material can improve the contact between the soil particles and increase the thermal conductivity [50] [74].
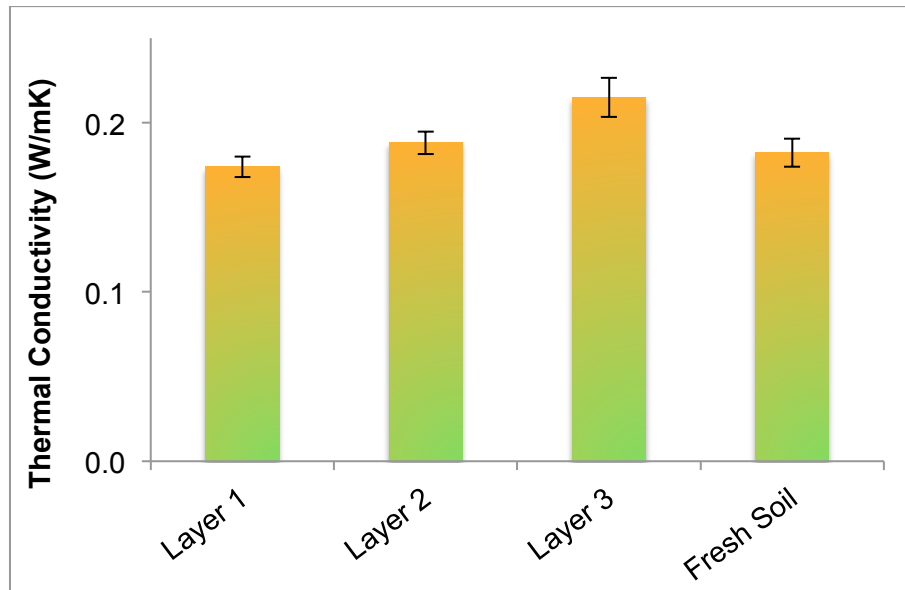
Figure 4.17: Thermal conductivity of each layer compared with the fresh media. The error bars are based on the 95% confidence interval of the mean.

Regarding the heat capacity (Figure 4.18) the trend is less obvious. For Layer 1 and Layer 2 there is no visible correlation, while Layer 3 has a statistically higher heat capacity. In comparison with the heat capacity of the fresh soil, Layer 3 is higher.
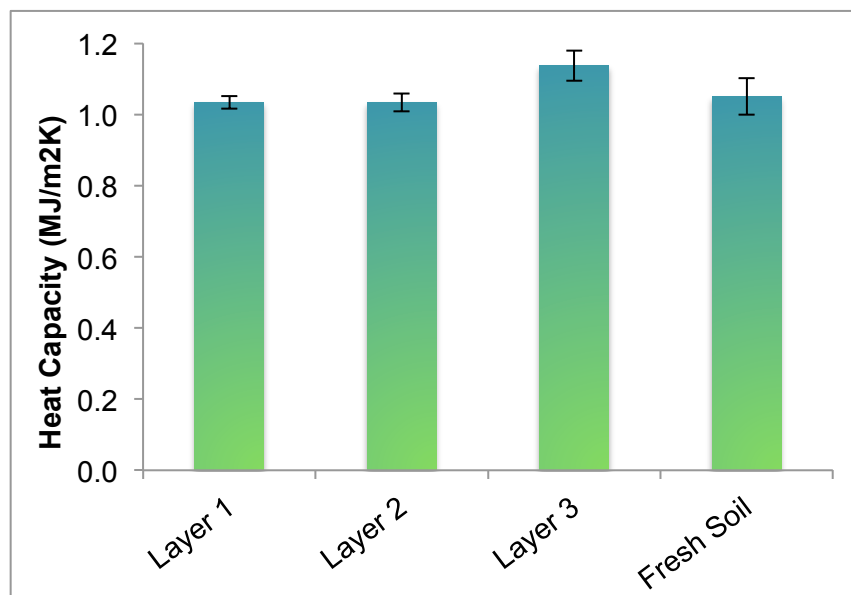
Figure 4.18: Volumetric heat capacity of each layer compared with the fresh media. The error bars are based on the 95% confidence interval of the mean.

In both cases, the 95% confidence interval was calculated based on the mean and considering each measurement (each of the nine samples has been tested three times).

It can then be concluded that changes in soil composition can affect the thermal characteristic of the green roof over time. The green roof module was taken from the roof one year after its installation, suggesting that changes in soil composition over one year can change the thermal properties. The measurements discussed above have been taken on dry soil.

4.3.2 Thermal Properties of Fresh Growth Media and Field Measurements (for different moisture contents)

As mentioned at the beginning of this section, the thermal properties have also been measured at different water contents to investigate the relationship between thermal properties and soil moisture. As described in Chapter 3, the laboratory measurements on fresh growth media have been conducted with two methodologies: the *beaker* and the *column* method. The measurements on the green roof site at Western University have been taken daily from June 18 to June 26, 2014. As illustrated in Figure 4.19, the green roof is made of separate modules on which three different plants species are grown: *grass*, *aquilegia* and *sedum*. The measurements have been taken on three different modules: one planted with grass (Figure 4.20, a), one with Aquilegia (Figure 4.20, b) and one bare module. The module vegetated with sedum was not tested because of the sensors could have been damaged due to the thickness of the vegetation and roots; moreover, the repeated insertion of the sensors could have damaged the roots system of the module. The bare module was installed on the roof at the beginning of June 2014 while the vegetated modules were two years old. The water content was measured with an EC-5 probe, connected to a datalogger (21X, Campbell Scientific) and the thermal properties were measured with the KD2 thermal properties analyzer. Both laboratory and field measurements are reported in Figure 4.21.

Figure 4.19: Green roof site at Western University (reproduced from [2]).
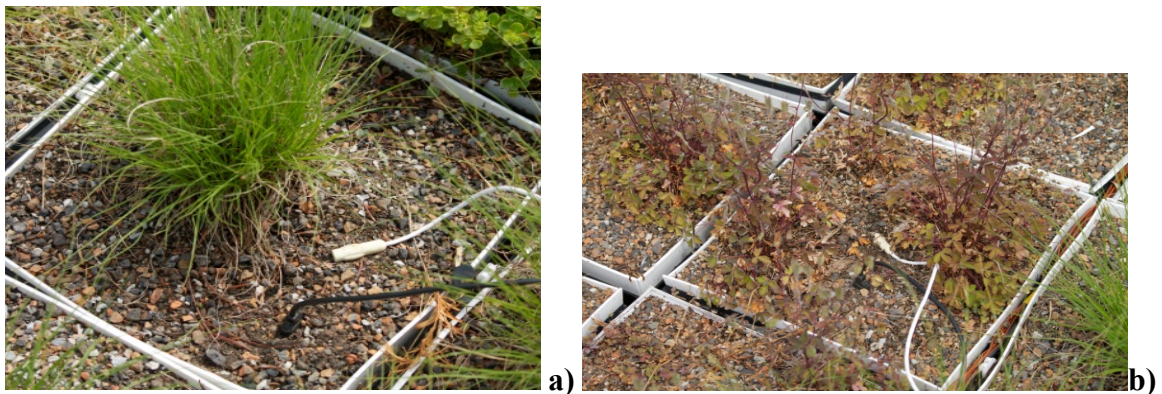
Figure 4.20: Field measurements of the soil thermal properties (with KD2 Pro) and water content (with EC-5) of green roof modules with *Grass* (a) and *Aquilegia* (b).

As described in Chapter 3, the measurements taken with the *beaker* method consist of three measurements per sample (the samples were three) at different water contents. The method allowed measuring the thermal conductivity up to $S_W = 0.7$, because at higher saturation levels the water partially migrated, due to gravity, to the bottom of the beaker, impacting the thermal readings. However, the range from 0 to 0.7 of water saturation is of more interest since 0.7 is usually the maximum water saturation reached in the field. As previously discussed, 0.7 represents the field capacity of the green roof.

As discussed in Chapter 2, the thermal properties of the soil can be estimated with the models described in the chapter that use the soil water content as input data. Four models

have been described: Johansen (JH), Côtè and Konrad (CK) [75], Lu et al. (LU) [76] and Sailor and Hagos (SH) [74]. In Figure 4.21 only the SH model (noted by the triangle-shaped markers) is reported because it doesn't require adjusting parameters.
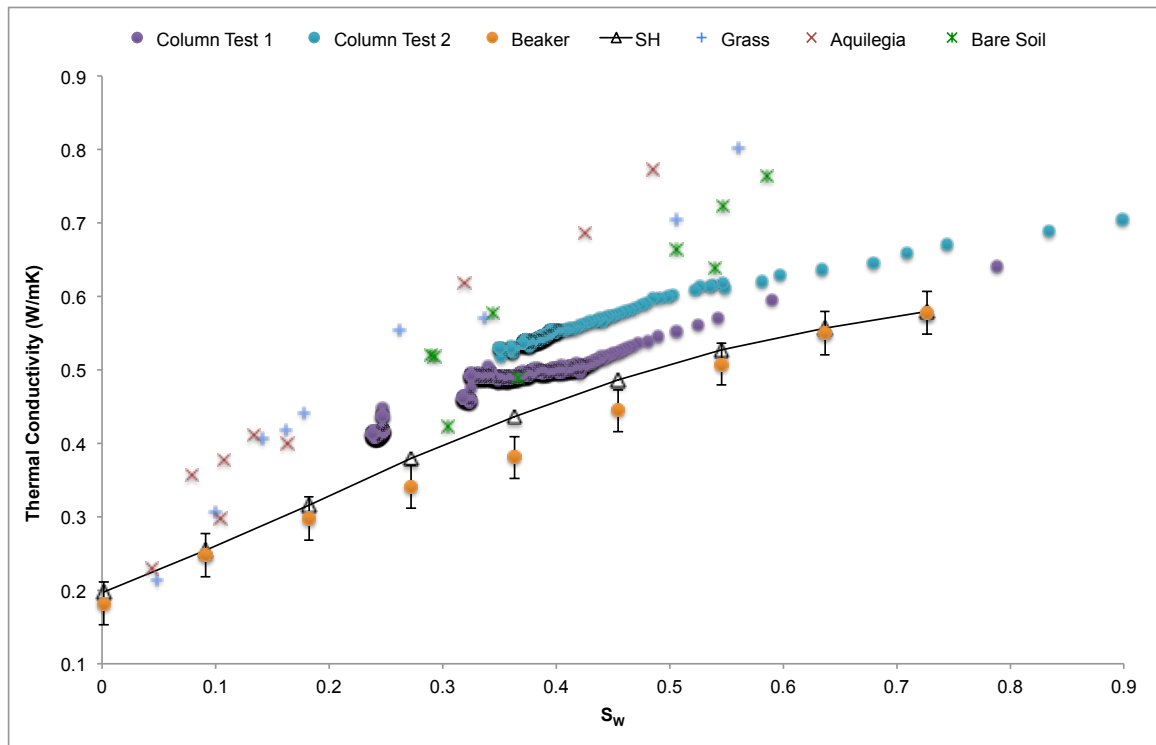
Figure 4.21: Thermal conductivity for different water saturation levels measured in the laboratory and on the field. In the chart, the black triangle-shaped markers represent the SH model (Sailor and Hagos) prior mentioned. The error bars represent the 95% confidence.

As expected, in all the experiments the thermal conductivity increases with the water content. However, from the results it can be noted that there is a difference between the thermal conductivity measured in the laboratory with the two methods and the thermal conductivity measured on the field.

First of all, it has to be pointed that laboratory and field conditions are different. In the laboratory, the average soil temperature ranges from 19°C to 22°C while on the field, even in morning when the measurements were taken, the soil temperature ranged from 20°C to 30°C and temperature can effect the readings of the sensors [67].

Secondly, regarding the two laboratory methods, the differences can be explained because with the *beaker* method, the soil is remixed at every change of the water content while in the *column* method the soil remains untouched for the experiment. Remixing the sample can lead to a lower compaction of the soil, therefore a lower range of thermal properties. Indeed, when the soil is less compacted, there are less contact points on the probe needles; also, when the saturation is higher than 0.5, the free water can more easily migrate downward to the bottom of the beaker. In agreement with these assumptions, both *column* data sets lie between the field measurements and the *beaker* measurements: they are lower than the filed measurements due to the reduced temperature and higher than the *beaker* measurements due to the higher compaction [74].

From Figure 4.21 it can also be noted that there is a difference between the types of module. Compared with *grass* and *aquilegia*, which have similar patterns, the bare soil presents more scattered data, as it can be also noted from the calculated R^2 in the following Table 4.6. This can be due to the fact that the bare soil was recently installed on the green roof, approximately two weeks before the measurements were taken. Therefore, the soil is less compacted than the two year-old *grass* and *aquilegia* modules. The difference in the field and the difference in the column are comparable, so they can also be due to the experimental methodology.

Table 4.6: R^2 of the field measured thermal conductivity and heat capacity from June 18 till June 26 (2014).

	Grass	Aquilegia	Bare Soil
R^2, Thermal Conductivity	0.95449	0.96642	0.82559
R^2, Heat Capacity	0.87483	0.90895	0.75857

Regarding the SH model, it can be noted that the model only estimates the *beaker* measurements reasonably well (RMSE = 0.0286). This can be explained by the fact that the method proposed by the authors was developed and tested with a methodology similar to the *beaker* method, where the soil is remixed every time the amount of water is changed.

The other three models (JH, CK, and LU) have been calibrated to fit measured field data. The calibration was done minimizing the RMSE of each model comparing the estimate and measured thermal conductivity. As described in Chapter 2, all the three models are based on the Kersten function of the JH model (eq. 2.17). In the equation, λ_{dry} (thermal conductivity of dry soil) and λ_{sat} (thermal conductivity of saturated soil) have been directly measured in the laboratory with the KD2 Pro and the values are 0.194 W/mk for dray soil and 1.004 W/mk for saturated soil. The parameter 0.7 of the JH model (eq. 2.18) was fitted to 0.97. Regarding the CK model [75], the authors say that the parameter h (eq. 2.19) can vary from 4.60 (for gravel and coarse sand) to 0.60 (for organic fibrous soils). For the field measurements reported here, the value that best estimates the measured thermal conductivity is 1.9. Finally, regarding the LU model, the values of the parameters (α and γ) originally proposed by the authors are 0.96 (for coarse textured soils) and 0.27 (for fine textured soils) for the parameter α and 1.33 for γ. The values of $\alpha = 0.78$ best estimates the field measurements while γ did not change. The calculated RMSE for each model are reported in Table 4.7

Table 4.7: RMSE for the JH, CK and LU models regarding the measured λ.

Model	JH	CK	LU
Parameter/s	0.97	h = 1.9	α = 0.78
RMSE	0.0564	0.0345	0.0445

The estimation of the thermal conductivity with the new corrected parameters is reported in Figure 4.22. In the figure two charts are shown; the first one illustrates the comparison between the measured thermal conductivity and estimated with the models. The second chart shows the measured and estimated water saturation plotted vs. the measured thermal conductivity. According to the RMSE for the fitted parameters and the charts in Figure 4.22, the models agree with the thermal conductivity of the green roof media reasonably well.
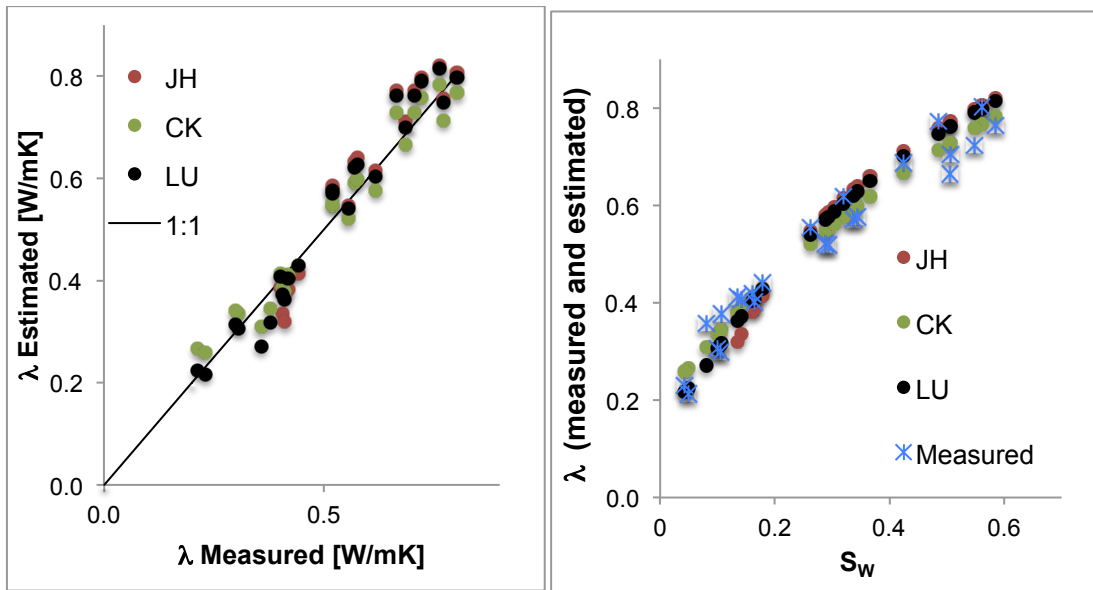
Figure 4.22: On the left, field-measured and estimated λ with the JH, CK and LU models. On the right, field-measured and estimated λ vs. S_W.

In Figure 4.23 the heat capacity measured in laboratory and on the field is reported; the legend of the chart is the same used for the chart in Figure 2.21 for the thermal conductivity.
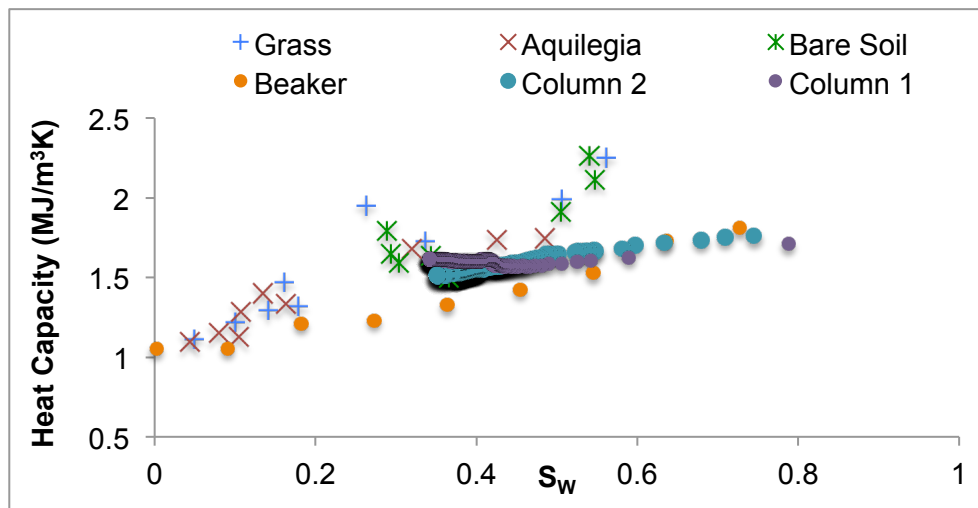
Figure 4.23: Heat capacity measured in the laboratory with the *beaker* and the *column* method and the heat capacity measured on the field.

From the chart, it can be noted that there is a qualitatively better agreement between the *column* and *beaker* method estimate of heat capacity than for the thermal conductivity. However, there is a quite large discrepancy between the field and laboratory measurements, especially for water saturation levels higher than 0.5. As mentioned before, external forcing, such as solar radiation and temperature, can affect the thermal properties and moisture readings. Indeed, it was observed in the laboratory and in the field, that the instrument readings are sensitive to temperature. In addition to this, there is another factor that has to be considered for the heat capacity. The green roof media consist mostly of porous particles, the expanded shale. These particles are capable of absorbing water over time and the longer the soil is in contact with water; the more the water can be absorbed. On the roof, the soil is always moist while during the laboratory experiments, the soil was completely dry before the experiments. Therefore, the particles on the roof can contain more water than the particles in the beaker or in the column.

4.3.2.1   Field measurements and heat flux equation

In Chapter 2 the one-dimensional heat flux equation is reported (eq. 2.8); if the heat flux (G) and the temperature gradient ($\partial T/\partial z$) are known, is then possible to calculate the thermal conductivity (λ).

On the same green roof site in London (ON), where the field measurements of the thesis have been taken, a heat flux plate and thermocouples are installed in one of the modules. The heat flux plate measures G (W/m^2) every 5 minutes 24/24 hours and the thermocouples measure the soil temperature at 1" and 4" from the surface with the same frequency. Whit this information is then possible to compare the thermal conductivity measured with the KD2 pro and the thermal conductivity calculated with eq. 2.8 and using the instrumental data from the roof.

The instrumental data considered refers to the data collected from June 18 till June 26 (2014) from 8:30am to 10:am, which are the same days and time during which the measurements with the KD2 Pro (discussed in the previous section) have been conducted. The comparison between the measured and calculated thermal conductivity is illustrated in the following Fig. 4.24
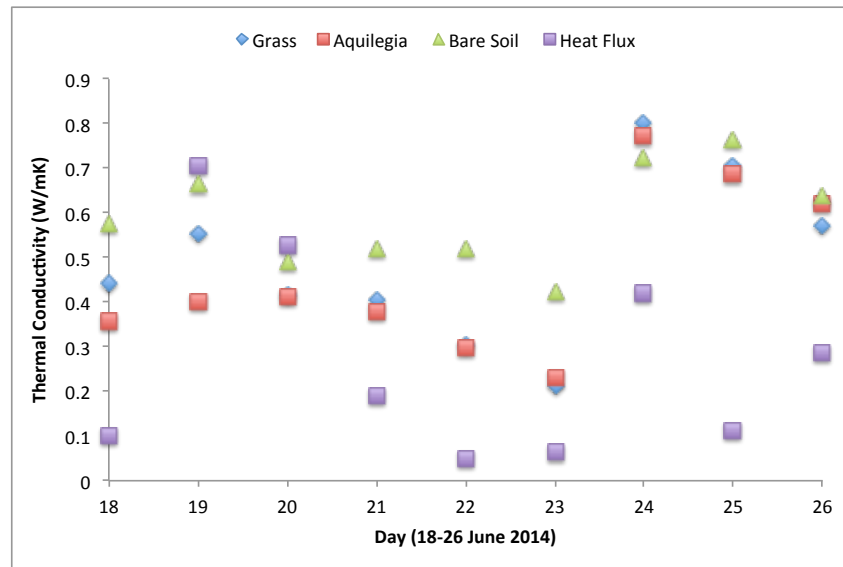
Figure 4.24: Comparison between the thermal conductivity measured with the KD2 Pro on the green roof module vegetated with Grass, Aquilegia and on bare soil and the thermal conductivity calculated with the heat flux eq. 2.8.

In the chart there are two peaks of thermal conductivity, on June 19 and June 24, this is because there were two rainfall events on the night of the previous day (respectively on June 18 and June 23). It can be noted that the thermal conductivity calculated with the heat flux, presents a range of values lower than the thermal conductivity measured on *grass, aquilegia* and bare soil. The only the exception is after the rainfall event occurred between 18 and 19 of June. One of the possible reason for the lower range of values is that *sedum*, that covers the module where are installed the heat flux plate and the thermocouples, has a thick vegetation coverage, therefore, the shades provided by the plants canopy is considerably higher than the shades provided by aquilegia and grass, in particular in that period when the measurements have been taken. Indeed, in the second half of June, grass and aquilegia were drier than sedum, because they just had the blooming season, while sedum was richer and approximating the blooming period. Therefore, the thicker vegetation coverage lowers the soil temperature and, as previously observed from the comparison between the laboratory and field measurements, when the temperature is lower, the thermal conductivity is also lower.

4.3.3   Estimation of Soil Water Content From the Thermal Inertia Approach

This paragraph presents the results of the estimation of the green roof water content through the thermal inertia approach. As discussed in Chapter 2, the approach is innovative and allows the characterization of the soil surface moisture though indirect measurements. Indeed, as a recall from Chapter 2, the soil water content is estimated through thermal images using the link between the thermal properties and the moisture content. The approach is relatively new to the small scale, especially to the green roof field and the thesis presents the initial step to test the applicability of the method to the green roof here analyzed. In Chapter 2 are discussed the studies conducted Maltese et al. in [51] and Manicapilli et al. in [53], which represent one of the first application of the small scale on soil module (not green roof) in laboratory conditions. At the university Politecnico di Milano (Italy) the thermal inertia technique is currently tested on the field for an extensive green roof. In this thesis the thermal images have not been utilized since the analyses presented here represent an initial stage to investigate the applicability of the method on the green roof soil using field measurements. The field measurements have been prior discussed in the section and they have been taken on three different modules: *grass*, *aquilegia* and bare soil.

As described in Chapter 2, with the thermal inertia approach, the water content can be derived from eq. 2.25 of Murray and Verhoef model (MV) [54] [53] according to eq. 2.26 recalled from Chapter 2:

$$\theta = \phi \left(1 - \frac{ln K_P}{\varepsilon}\right)^{1/-\mu} \qquad\qquad 2.26$$

The objective consists of estimating the water content of the green roof modules (grass, aquilegia and bare soil) using the thermal properties measured fore the same modules. The set of field measurements is the same earlier discussed in the section. The thermal properties are used to calculate K_P using eq. 2.24 here recalled:

$$P = K_P(P_{SAT} - P_{DRY}) + P_{DRY} \qquad\qquad 2.24$$

Where P_{SAT} and P_{DRY} have been calculated using the thermal properties measured in the laboratory on saturated and dry soil. With the second stage of the analysis that is not investigated in the thesis, the water content will be estimated with the thermal inertia obtained from remote sensed thermal images.

For comparison reasons, the MV model is also compared with the JH, CK and Lu models prior discussed. Regarding the JH model, the water content can be derived from eq. 2.18 as follows:

$$\theta = \phi 10^{((K_e - 1)/0.97)} \qquad 4.2$$

While for the CK model the water content can be derived from eq. 2.19 as follows:

$$\theta = \phi \frac{K_e}{h + (1 - h)K_e} \qquad 4.3$$

Finally, for the LU, the water content is derived form eq. 2.20 as follows:

$$\theta = \phi^{(\alpha - 1.33)} \sqrt{\alpha - lnK_e} \qquad 4.4$$

The parameters of the three models are the same that have been presented in Table 4.7. The parameters of the MV model (ε and μ) have been fitted in the same way, minimizing the RMSE and the values are respectively 3.7 and 0.18 (for the three types of green roof module). The comparison between the MV model and the other three models is reported in the following Fig. 4.25. The figure presents on the y-axis the water saturation estimated with MV, JH, CK, LU models and on the x-axis the measured values.
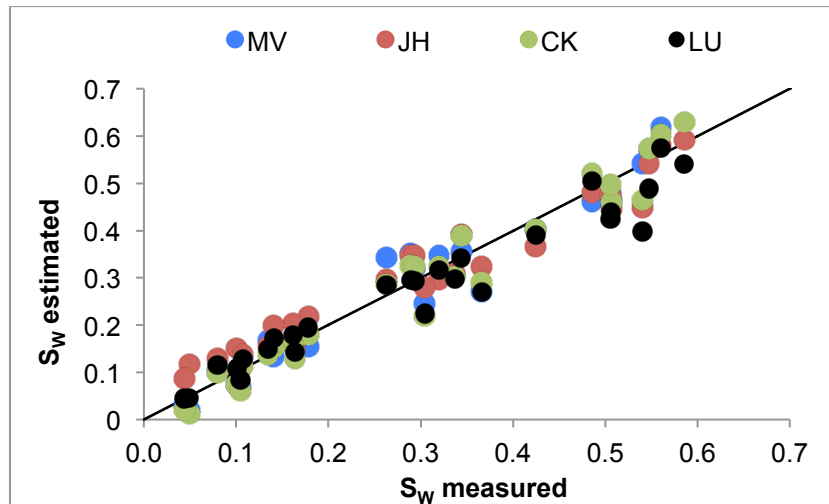
Figure 4.25: Comparison between the measured water content (expressed as water saturation, S_W) and the water content estimated with the models: MV, CK, and LU.

The following Figure 4.26 presents on the y-axis the thermal inertial, which was calculated with the values of measured thermal properties; on the x-axis presents the water saturation, which was estimated with the four models, and the water saturation that was measured in the field
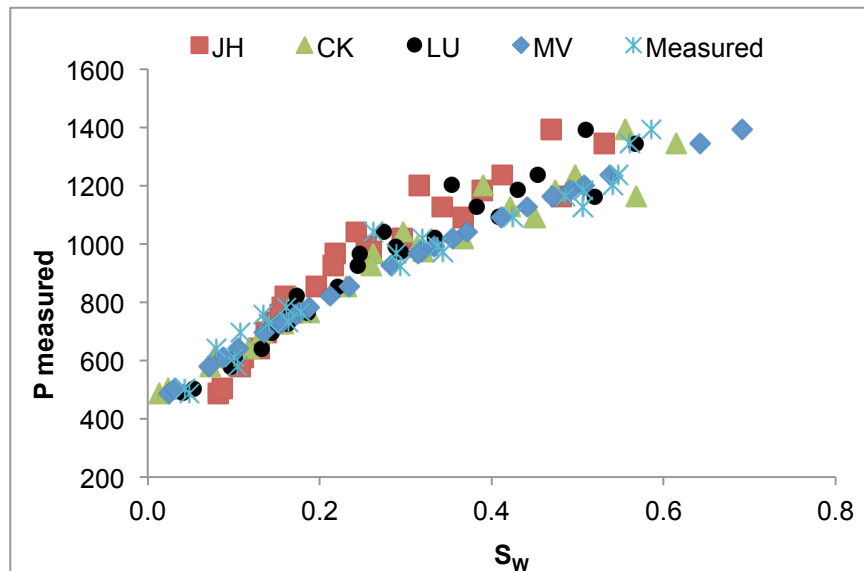
Figure 4.26: Comparison between the water content (measured and estimated) and the thermal inertia P calculated with measured thermal properties.

In the following Figure 4.27, the values of water saturation presented in Figure 4.26 have been converted into volumetric water content in order to compare the results with the studies presented by [52] [53]. As the two figures show, the analyses conducted on the green roof of London (ON) present range of values similar to the results reported by Manicapilli et al. in [53] on clay loam soil. According to these results it can then be assumed that the method is also applicable to the green roof growth media and the fitted parameters for the MV model correctly estimate the water content, in agreement with the previously discussed models (JH, CK, LU).
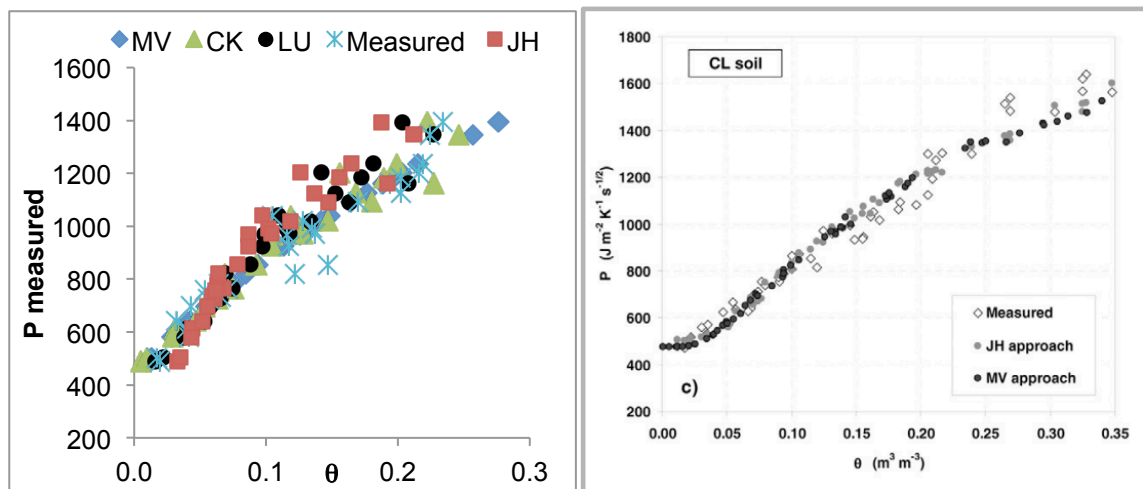
Figure 4.27: Comparison between the results of the thesis and the study published by Manicapilli et al. [53](the chart on the right is reproduced from [53])

Chapter 5 – Summary and Conclusion

5   Introduction

This chapter presents the summary and the conclusion of the thesis. The thesis contributions and the opportunities for future work are also discussed.

5.1   Conclusion

According to the results on the soil composition and sieve analyses, it can be concluded that the fines content of the media has a strong influence on the SWRC. Indeed, the presence of the fines particle contributes to the increment in the field capacity of the soils, which is fundamental for the green roof stormwater management performances. These fines have been observed to decrease over one year, during which the media was exposed to the outdoor environment on the roof and supported the plants. It was observed that the content of fines in the surface layer of the module was approximately half than the content of fines in the fresh soil. A possible solution to face this problem could be to change the composition of the fine material (for instance, by providing lighter fines than the limestone) or to change the design of outlet of the drainage system to avoid the fines passing through the apertures. When it was attempted to replicate the fines loss in the laboratory by flushing the soil with water in the pressure cell, it was observed that even if the sample was flushed with an amount of water higher than the average precipitation in London (ON), the mass loss was lower than the mass loss observed in the field. This can be explained because the outlet of the pressure cell consists of only one narrow opening while the green roof module has larger and more openings.

In addition to the changes of the fines content, it was also observed that, in the long term, the growth media presented changes in the organic content that decreased in the lower layer of the media in comparison with the fresh soil. As observed in the laboratory analyses (and confirmed in the literature of the soil science), changes in the organic content can affect the thermal behavior of the soil. The reduced organic content can reduce the insulation of the media, thereby, increasing the thermal properties.

Regarding the characterization of the hydraulic properties of the media, the experimental analyses of the thesis focused on both saturated and unsaturated soil. For the saturated hydraulic conductivity, three methodologies were presented and discussed. The first two methods are commonly applied on natural/standard soils; however, it was observed that they did not provide consistent and repeatable results for the growth media. Therefore, in the thesis, a third method was developed, specifically for the type of green roof soil that successfully measured the hydraulic conductivity.

The study of unsaturated soil properties (SWRC) represented the main focus of the thesis, since unsaturated conditions are the most common in green roofs. The thesis reports the study of primary curves and scanning curves of imbibition and drainage tests on fresh soil. From the drainage tests, it was possible to measure the field capacity of the soil and the laboratory results confirmed the data collected in the field. The Van Genuchten model was then applied to estimate the water content of the laboratory tests for the drainage curve and the curve after the drainage, where the water loss is due to evaporation. As discussed in Chapter 4, it is advisable that the parameters of the VG model presented in the thesis should be applied with caution for further modeling. First of all, the parameters fitted for the curves for the water loss due to evaporation need to be considered more carefully. As discussed in Chapter 4, the VG model is not supposed to describe the SWRC for the evaporation. Another observation to take into consideration for the application of the VG parameters is the less accuracy of the model for the initial part of the drainage curve. The parameter α that represent the inverse of the entry pressure overestimates the experimentally measured entry pressure for the green roof media. An overestimation of the entry pressure suggests that the soil drains faster compared to the estimated value and this can influence the understanding of the green roof behavior and the modeling. Regarding the comparison of the laboratory experiments of the water loss with the field observations, it is necessary to take into consideration that the duration of the drainage is faster in the field than in the laboratory because of the different design of the outlet. In both cases (laboratory and field), the water loss due to evaporation involves several days; therefore, the modeling for that region of the SWRC has to be more

carefully considered. Taking into consideration the limitations of the VG model, it was possible to successfully estimate the capillary pressure in the filed using the VG parameters calculated only for the drainage curves.

Regarding the characterization of the thermal properties of the media, the thesis provided values of the thermal conductivity and heat capacity for both fresh and used soil. The thermal properties measured in thesis can provide a useful comparison for the other studies ongoing in the greed roof project. Indeed, the measurements conducted in the thesis provided not only the values of the thermal parameters, but also the other environmental conduction and variable such as moisture content, compaction, organic content and temperature. In particular, the fitted parameters for three different models are provided that relate the thermal conductivity to the soil water content. These fitted parameters are useful for further studies in the field. As additional support to the laboratory and field measurements, the thermal conductivity measured with the thermal properties analyzer KD2 Pro was also compared to the thermal conductivity measured using the heat flux and the temperature gradient obtained from the instrumental measurements on green roof. The comparison highlighted the important effect of a different vegetation cover on the thermal properties of the soil. From the comparison, it was also possible to observe the similarity in the relationship with the water content among all the vegetation types. Finally, during the first stage of the application of the thermal inertia approach, it was possible to calibrate the parameters of the MV model and correctly estimate the soil water content for three different green roof modules (grass, aquilegia and bare soil). The results support further applications of the thermal inertia methodology for the green roof field.

5.2   Thesis Contribution

This section summarizes which are the contributions of this work.

- This study provides useful input parameters that can be applied for the green roof numerical model of the project, as stated in the aim of the thesis. The results can also be useful for the other ongoing studies in the green roof project.

- The comparison between fresh and used soil allowed a deeper understanding of which processes are happening on the roof and what it could be expected in the long term.

- The thesis offers a set of methodologies and procedures that can be applied to other green roof growth media for future analyses.

- The thesis presents and discusses the best methodologies to characterize soil properties of difficult materials such as the growth media that is highly, heterogeneous and contains lightweight expanded materials, clay and organic matter.

5.3   Future Work

This section indicates which are the possible analyses that can extend the work here presented.

First, the same analyses that have been conducted on the one-year old soil can be repeated on a two-year old soil (vegetated with the same plant species, *sedum*). This will allow a further understanding of the physical processes and changes ongoing on the green roof.

Second, according to the fact that the soil loses the fines particles over time, a new type of mixture can be tested, substituting the heavy fine particles of the limestone with lighter ones. This means that the limestone used in the new soil mixture will consist only on coarse particles.

Bibliography

[1] J. Mentens, D. Raes, and M. Hermy, "Green roofs as a tool for solving the rainwater runoff problem in the urbanized 21st century?," *Landscape and Urban Planning*, vol. 77, pp. 217-226, 2006.

[2] Restore. (2012) RESTORE: Research for Subsurface Transport and Remediation. [Online]. www.eng.uwo.ca

[3] LiveRoof. LiveRoof. [Online]. http://liveroof.com/

[4] B. Bass, S.S. Alcazar R. Martens, "Roof-envelope ration impact on green roof energy performance," *Urban Ecosyst* , vol. 11, pp. 399-408, April 2008.

[5] K. Metselaar, "Water retention and evapotranspiratin of green roofs and possible natural vegetation types ," *Resources, Conservation and Recycling* , vol. 64, pp. 49-55, 2012.

[6] EPA. (2011, December) EPA. [Online]. www.epa.gov

[7] D.J. Sailor, D. Hutchinson, and L. Bokovoy, "Thermal property measurements for ecoroof soils common in the western U.S.," *Energy and Buildings*, pp. 1246–1251, 2007.

[8] S.-E. Ouldboukhitine, R. Belarbi, and R. Djedjig, "Characterization of green roof components: Measurements of thermal and hydrological properties," *Building and Environment*, pp. 78-85, 2012.

[9] S.S. Moody and D.J. Sailor, "Development an application of a building energy performance metric for green roof systems," *Energy and Building*, vol. 60, pp. 262-269, 2013.

[10] E. A. Voyde, "Quantifying the Complete Hydrologic Budget for an Extensive Living Roof," 2011.

[11] P.A.Y. Ampim, J.J. Sloan, R.I. Cabrera, D.A. Harp, and F.H. Jaber, "Green roof growing media: Types, ingredients, composition and properties," *Journal of Environmental Horticulture*, vol. 28, no. 4, pp. 244-252, Jan 2010.

[12] D.J. Sailor and M. Hagos, "An updated and expanded set of thermal property data for green roof growing media," *Energy and Buildings*, pp. 2298–2303, 2011.

[13] E. E. Fassman and R. Simcock, "Moisture Measurements as Performance Criteria for Extensive Living Roof Substrates," *Journal of Environmental Engineering*, vol. 138, pp. 841-851, August 2012.

[14] R.D. Stoll and T.A. Holm, "Expanded shale lightweight fill: geotechnical properties," *Journal of Geotechnical Engineering* , vol. 111, no. 8, pp. 1023-27 , 1985.

[15] S. L. Dingman, *Physical Hydrology* , Second Edition ed. Long Grove , Illinois : Waveland Press, Inc. , 2008.

[16] M.R. Hendriks, *Introduction to Physical Hydrology*. New York, USA: Oxford University Press Inc., 2010.

[17] The Landscape Development and Landscaping Research Societt e.V. - (FLL), FLL: Guideline for planning, construction and mantainance of green roofing, 2008.

[18] A. Palla, I. Gnecco, and L.G. Lanza, "Unsaturated 2D modelling of subsurface water flow in the coarse-grained porous matrix of a green roof," *Journal of Hydrology*, vol. 379, pp. 193-204, 2009.

[19] A. Palla, I. Gnecco, and L.G. Lanza, "Compared performance of a conceptual and

mechanistic hydrologic models of a green roof," *Hydrological Processes*, vol. 26, pp. 73-84, 2012.

[20] E.A. Fassman, "Effect of roof slope and substrate depth on runoff," in *Greening rooftops for sustainable communities, conference awards and trade show.*, Baltimore, 2008.

[21] M. Fiori and R. Paolini, "Green Roof Report," University Politecnico di Milano, Milan, 2013.

[22] A. Nagase and D. Dunnett, "Amount of water runoff from different vegetation types on extensive green roofs: effects of plant species, diversity and plant structure," *Landscape and Urnam Planning*, vol. 104, pp. 356-363, 2012.

[23] D.J. Babilis and P.A. Londra, "Assessment of various methods for the determination of hydraulic conductivities of two green roof substrates by steady state infiltration experiments," *Irrigation and Drainage*, vol. 60, pp. 274-280, 2011, wileyonlinelibrary.com.

[24] E. Voyde, E. Fassman, and R. Simcock, "Hydrology of an extensive living roof under sub-tropical climate conditions in Auckland, New Zealand," *Journal of Hydrology*, no. 394, pp. 384-395, 2010.

[25] D.J. Bond and G.W.H. Thompson, "Flow modelling in green roof systems," University of Canterbuty, Christ Church (NZ), Final Year Project 2013.

[26] J.C. DeNardo, A.R. Jarrett, H.B. Manbeck, D.J. Beattle, and R.D. Berghage, "Stormwater mitigation and surface temperature reduction by green roofs," *American Society of Agricultural Engineers*, vol. 48, no. 4, pp. 1491-1496, June 2005.

[27] S. Zhang and Y. Guo, "Analytical probabilistic model for evaluating the hydrologic performance of green roofs," *Journal of Hydrologic Engineering*, vol. 18, no. 1,

January 2013.

[28] C.W. Fetter, *Contaminant Hydrology*, Second Edition ed. Upper Saddle River, New Jersey, US: Prentice Hall, 1999.

[29] A. Wayllace and N. Lu, "A transient water release and imbibitions method for rapidly measuring wetting and drying soil water rentetion and hydraulic condictivity functions," *Geotechnical Testing Journal*, vol. 35, no. 1, 2013, www.astm.org.

[30] M. Mavroulidou, Z. Cabarkapa, and M.J. Gunn, "Efficient laboratory measurements of the soil water retention curve," *Geotechnical Testing Journal*, vol. 36, no. 1, 2013, available online at www.astm.org.

[31] W.J. Rawls, Y.A. Pachepsky, J.C. Ritchie, T.M. Sobecki, and H. Bloodworth, "Effect of soil organic carbon on soil water retention," *Geoderms*, vol. 116, pp. 61-76, 2003.

[32] G. W. Camps-Roach, "Investigating the transient of two-phase flow in porous media," University of Western Ontario , London (ON), Master of Engineering Science 2008.

[33] B. Ghanbarian-Alavijeh, A. Liaghat, H. Guan-Hua, and M.T. Van Genuchten, "Estimation of the van Genuchten soil water retention properties from textural data," *Pedosphere*, vol. 20, no. 4, pp. 456-465, 2010.

[34] L. Guarracino, "Estimation of saturated hydraulic conductivity Ks from the van Genuchten shape paramter alpha," *Water Resource Research* , vol. 43, 2007.

[35] V.G. Aschonitis and V.Z. Antonopoulos, "New equations for the determination of soil saturated hydraulic conductivtiy using the van Genuchten model paramters and effective porosity," *Irrigation and Drainage*, vol. 62, pp. 537-542, 2013.

[36] X. Yang and X. You, "Estimating parameters of van Genuchten model for soil water

retentioncurve by intelligent algorithms," *Applied Mathematics & Information Sciences*, vol. 7, no. 5, pp. 1977-1983, 2013.

[37] Y. Guo, S. Zhang, and S. Liu, "Runoff reduction capabilities and irrigation requirements of green roofs," *Water Resour Manage*, vol. 28, pp. 1363-1378, 2014.

[38] R. Hilten, An analysis of the energetics and stormwater mediation potential of green roofs, 2002, Thesis of Master of Science, University of Georgia.

[39] T.E. Ochsner, R. Horton, and T. Ren, "A New Perspective on Soil Thermal Properties," *SSSAJ*, vol. 65, pp. 1641-1647, 2001.

[40] N.H. Abu-Hamdeh and R.C. Reeder, "Soil Termal Conductivity: Effects of Density, Moisture, Salt Concentration, and Organic Matter," *SSSAJ*, vol. 64, pp. 1285-1290, 2000.

[41] M.P. Deru, "Ground-Coupled Heat and Moisture Transfer from Buildings Part 1: Analysis and Modeling," in *(ASES) National Solar Conferences Forum 2001*, Washington, D.C., 2011.

[42] S.R. Evett, N. Agam, W.P. Kustas, P.D. Colaizzi, and R.C. Schwartz, "Soil profile method for soil thermal diffusivity, conductivity and heat flux: comparison to soil heat flux plates," *Advances in Water Resources*, vol. 50, pp. 41-54, 2012.

[43] S. Lu, T. Ren, T. Gong, and R. Horton, "An improved model for predicting soil thermal conductivity from water content at room temperature," vol. 71, pp. 8-14, 2006.

[44] O.T. Farouki, *Thermal Properties of Soils*.: Trans Tech, 1986, vol. 11 (1986).

[45] Z. Ju, T. Ren, and C. Hu, "Soil thermal conductivity as influenced by agrregation at intermediate water contents," *SSSAJ*, vol. 75, pp. 26-29, 2010.

[46] B. Usowicz and L. Usowicz, Thermal conductivity of soils: comparison of experimental results and estimation methods.

[47] F. Oliver. (2000) Institute of Atmospheric and Climate Change at ETH (Eidgenössische Technische Hochschule Zürich). [Online]. www.iac.ethz.ch

[48] K.L. Bristow, G.J. Kluitenberg, C.J. Goding, and T.S. Fitzgerald, "A small multi-needle probe for measuring soil thermal properties, water content and electrical conductivity," *Computer and Electronics in Agriculture*, vol. 32, pp. 265-280, 2001.

[49] J. Côté and J.-M. Konrad, "A generalized thermal conductivity model for soils and construction materials," *Canadian Geotechnical Journal*, vol. 42, no. 2, pp. 443-458, 2005.

[50] D.J. Sailor, "A green roof model for building energy simulation programs," *Energy and Buildings*, vol. 40, pp. 1466-1478, 2008.

[51] M. Manicapilli, C. Cammalleri, G. Ciraolo, F. D'Asaro A. Maltese, "A thermal inertia model for soi water content retrieval using thermal and multispectral images," *Remote Sensing fo Agriculture, Ecosystem and Hydrology XII*, vol. 7824, no. 78241G-1, 2010.

[52] C. Cammalleri, G. Ciraolo, F. D'Asaro, A. Maltese M. Manicapilli, "Un modello di inerzia termic per la stima del contenuto idrico del suolo da immagini termiche e multispettrali.," in *XXXII Convegno Nazionale di Idraulica e Costruzioni Idriche*, Palermo, 2010, pp. 14-17.

[53] C. Cammalleri, G. Ciraolo, F. D'Asaro, A. Maltese M. Manicapilli, "Thermal inertia modelling for soil surface water content estimation: a laboratory experiment," *Soil Physics*, vol. 76, no. 1, pp. 92-100, Jan-Feb 2012.

[54] A. Verhoef T. Murray, "Moving towards a more mechanistic approach in the

determination of soil heat flux from remote measurements II. Diurnal shape of soil heat flux," *Agricultural and Forest Meteorology* , vol. 147, pp. 88-97, June 2007.

[55] R. Paolini M. Fiori, "Green Roof Report," University Politecnico di Milano, Milan, 2013.

[56] Z. Ju, T. Rena, R. Horton S.Lu, "A general approach to estimate soil water content from thermal inertia," *Agricultural and Forest metereology*, vol. 149, pp. 1693-1698, May 2009.

[57] Greenroofs.com. Greenroofs.com. [Online]. http://www.greenroofs.com

[58] G. Goel, "Experimental investigation of dynamic effects in capillary pressure: fluid property effects," University of Western Ontario, London (ON), Master Engineering Scince 2010.

[59] G.W. Camps-Roach, D.M. O'Carroll, T.A Newson, T. Sakaki, and T.H. Illangasekare, "Experimental investigation of dynamic effects in capillary pressure: grain size dependency and upscaling," *Water Resources Rsearch*, vol. 46, p. W08544, 2010.

[60] D.M. O'Carroll and G.W. Goel, "Experimental Investigation of nonequilibrium capillarity effects: fluids viscosity effects," *Water Resources Research*, vol. 47, p. W09507, 2011.

[61] T. Sakaki, A. Limsuwat, K.M. Smits, and T.H. Illangasekare, "Empirical two-point α-mixing model for calibrating the ECH2O EC-5 soil moisture sensor in sands," *Water Resources Research*, p. VOL. 44, 2008.

[62] K.M. Smits, T. Sakaki, S.T. Howington, J.F. Peters, and T.H. Illangasekare, "Temperature dependence of thermal properties of sands across a wide range of temperatures," *Vadose Zone Journal*, vol. 2, no. 1, pp. 1-8, 2012.

[63] D. Kurukula, A Comparison of the Energy Balance of Green Roofs in Calgary, Alberta and London, Ontario , 2013.

[64] D.M. O'Carroll, T.J. Phenal, and L.M. Abriola, "Exploring dynamic effects in capillary pressure multistep outflow experiments," *Water Resources Research*, p. VOL.41, 2005.

[65] D. M. O'Carroll, and T. Illangasekare T. Sakaki, "Direct quantification of dynamic effects in capillary pressure fro drainage-wetting cycles," *Vadose Zone*, pp. 422-437, 2010.

[66] PENNSTATE, Agricultural Analytical Services Laboratory.

[67] Inc. Decagon Devices, Ed., *KD2 Pro, User Manual*, 6th ed., 2008.

[68] J.I. Gerhard, "DNAPL infiltration, redistribution and immobilization in porous media," Civil Engineering, Kingston, Ontario Canada, Queen's University, Kingston, Ph. D. Thesis 2002.

[69] Environment Canada. Meteorological Service of Canada. Canadian Climate Normals. [Online]. climate.weather.gc.ca

[70] L. Guarracino, "Estimation of saturated hydraulic conductivity Ks from the van Genuchten shape parameter alpha," *Water Resources Research*, vol. 43, 2007.

[71] V.G. Aschonitis and V.Z. Antonopoulos, "New Raquation for the determination of soil saturated hydraulic conductivity using the Van Genuchten model parameters and effective porosity," *Irrigation and Drainage*, vol. 62, pp. 537–542, 2013.

[72] R.F. Carsel and R. Parrish, "Developing joint probability distributions of soil water retention characteristics," *Water Resources Research*, vol. 24, no. 5, pp. 755-769, May 1988.

[73] G.C. Topp, "Soil water hysteresis in silt loam and clay loam soils," Depart ment of Agriculture, Soil Research Institute, Ottawa,.

[74] D. J. Sailor and M. Hagos, "An updated and expanded set of thermal property data for green roof growing media," *Energy and Buildings*, pp. 2298–2303, 2011.

[75] J.-M. Konrad J. Côté, "A generalized thermal conductivity model for soils and construction materials," *Canadian Geotechnical Journal*, vol. 42, no. 2, pp. 443-458, 2005.

[76] T. Ren, T. Gong, and R. Horton S. Lu, "An Improved Model for Predicting Soil Thermal Conductivity from Water Content at Room Temperature," vol. 71, pp. 8-14, 2006.

[77] T Sakaki, A. Limsuwat, and T.H. Illangasekare, "A simple method for calibrati ng dielectric soil moisture sensors: laboratory validati on in sands," *Vadose Zone Journal*, vol. 10, pp. 526-531, Mar. 2011.

[78] D.M. O'Carroll and B.E. Sleep, "Hot water flushing for immiscible displacement of a viscous NAPL," *Journal of Contaminant Hydrology*, vol. 91, pp. 247-266, 2007.

[79] U.S. Geological Survey. USGS, Science for a changing world. [Online]. www.usgs.gov

[80] K.M. Smits, T. Sakaki, S.E. Howington, J.F. Peters, and T.H. Illangasekare, "Temperature dependence of thermal properties of sands across a wide range of temperatures (30–70°C)," *Vadose Zone Journal*, vol. 12, no. 1, pp. 1-8, Mar. 2012.

[81] K. L. Bristow, "Measurement of thermal properties and water content of unsaturated sandy soil using dual-needle heat-pulse probes," *Agricultural and Forest Meterology* , vol. 89, pp. 75-84, August 1998.

[82] A Al-Busaidi, T. Yamamoto, S. Tanak, and Moritani S., *Evapotranspiration of Succulent Plant (Sedum aizoonvar.floibundum)*, Dr. Stavros G. Alexandris (Ed.), ISBN: 978-953-51-1115-3, InTech, DOI: 10.5772/53213. Evapotranspiration - An Overview, Ed., 2013, vol. 12, Available from: http://www.intechopen.com/books/evapotranspiration-an-overview/evapotranspiration-of-succulent-plant-sedum-aizoonvar-floibundum-. [Online]. http://cdn.intechopen.com/pdfs-wm/40958.pdf

[83] A. Tarantino, E. Romero, and Y.J. Cui, *Laboratory and Field Testing of Unsaturated Soils.*, 2008, vol. 26.

[84] K. Rajkaia, S. Kabos, and M.T. Van Genuchten, "Estimating the water retention curve from soil properties: comparison of linear, nonlinear and concomitant variable methods," *Soil & Tillage Research*, no. 79, pp. 145-152, 2004.

[85] R.M. Nagare, R. A. Schincariol, W. L. Quinton, and M. Hayashi, "Laboratory calibration of time domain reflectometry to determine moisture content in undisturbed peat samples," *European Journal of Soil Science*, pp. 505-515, 2011.

[86] Decagon Devices, Frequently Asked Questions about the Decagon's Soil Moisture Probes and Accessories, 2009 , support@decagon.com.

[87] A. Palla, I. Gnecco, and L.G. lanza, "Unsaturated 2D modelling of subsurface water flow in the coarse-grained porous matrix of a green roof," *Journal of Hydrology*, vol. 379, pp. 193-204, 2009.

[88] P. Breach, Evapotranspiration of a Green Roof in Calgary, Alberta, 2014, Civil Engineering B.Sc. Final Report, Western University.

[89] H.P. Cresswell, T.W. Green, and N.J. McKenzie, "The adequacy of pressure plate apparatus for determining soil water retention," *SSSAJ*, vol. 72, no. 1, pp. 41-49, Jan/Feb 2008.

[90] S.S. Alcazar and B. Bass, "Energy performance of green roofs in a multi storey residential building in Madrid," in *Greening rooftops for sustainable communities.*, Washington, 2005.

[91] S. Lu, Z. Ju, T. Ren, and R. Horton, "A general approach to estimate soil water content from thermal inertia," *Agricultural and Forest meteorology*, vol. 149, pp. 1693-1698, May 2009.

[92] D.B. Stephens, *Vadose Zone Hydrology*.: CRC Press, Inc., 1996.

[93] M. Manicapilli, C. Cammalleri, G. Ciraolo, F. D'Asaro, and A. Maltese, "Thermal inertia modelling for soil surface water content estimation: a laboratory experiment," *Soil Physics*, vol. 76, no. 1, pp. 92-100, Jan-Feb 2012.

[94] A. Maltese, M. Manicapilli, C. Cammalleri, G. Ciraolo, and F. D'Asaro, "A thermal inertia model for soil water content retrieval using thermal and multispectral images," *Remote Sensing fo Agriculture, Ecosystem and Hydrology XII*, vol. 7824, no. 78241G-1, 2010.

Appendices

Appendix A: Calibration Methodologies

Calibration of the Pressure Transducers

The pressures transducers (FP2000, Honeywell, Columbus, OH. USA) are connected to the data-logger (CR7, Campbell Scientific, Logan, Utah) and they measure the water pressure inside the soil chamber. The readings are recorded in mV and they can be converted in the corresponding pressure in centimeters of water with the calibration coefficients.

The calibration consists of a simple method; the pressure transducers are connected to a graduated burette in which is injected D.I. water. The water level inside the burette varied from 30 to 20 and 10 cm. At each water level corresponded a certain mV reading for the pressure transducers. Therefore, it is possible to find the calibration coefficients (slope and intercept) for the linear relationship between the data-logger readings and the water level in the burette (in cm of water). In Table A-I are reported the values of the calibration tests for six pressure transducers (a second pressure cell with another set of three pressure transducers was built).

Table A - I: Calibration data for the six pressure transducers.

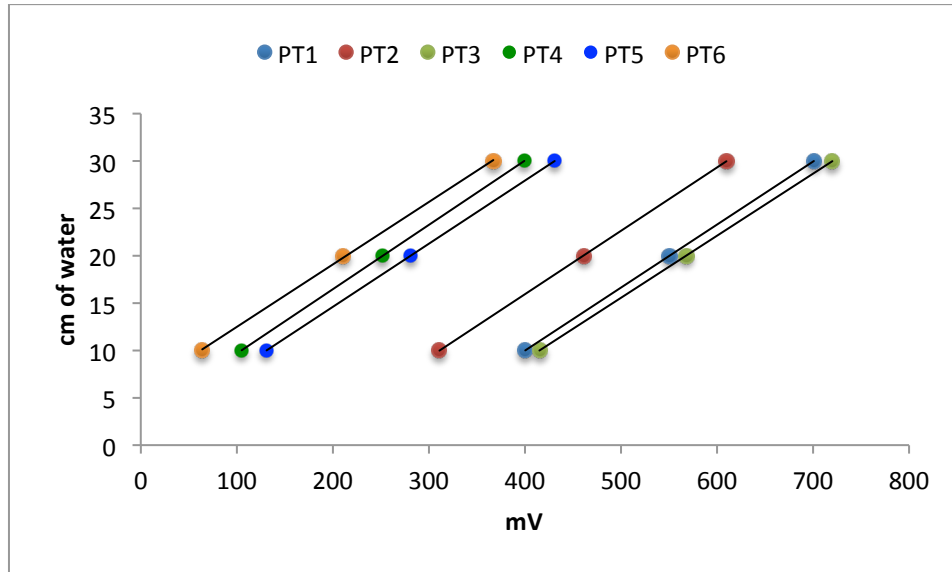| Cm of water	PT1	PT2	PT3	PT4	PT5	PT6
30	700.87	609.83	720.15	399.40	431.00	367.09
20	550.41	461.21	568.01	251.50	280.76	210.60
10	400.36	311.01	415.09	105.05	131.00	64.00
Slope	0.0666	0.0669	0.0656	0.0679	0.0667	0.0660
Intercept	-16.64	-10.83	-17.22	2.88	1.27	5.89

Figure A - I: Calibration curves for the six pressure transducers.

Calibration of the EC-5s

To calibrate the moisture sensors EC-5, it was adopted the two-point method proposed by Sakaki et al. in [61]:

$$\theta = \frac{ADC^\alpha - ADC_{dry}{}^\alpha}{ADC_{sat}{}^\alpha - ADC_{dry}{}^\alpha} \, \phi$$

Where θ is the volumetric water content, ϕ is the porosity of the soil and *ADC* represents the digital counts that, for the ECH₂O moisture sensor EC-5, can be calculated [77] as follows:

$$ADC = [mV] \times 1.3661$$

The parameter α has a value of 2.5; specific for the ECH₂O EC-5, and it was obtained based on the ADC values in the study conducted by [61], during which the authors tested 30 EC-5 moisture probes.

As previously done by [32], the calibration of the EC-5s is done inside the soil chamber, in order to minimize any interference with the aluminum cell. The two points for dry and

saturated soil are taken during the wetting of the soil sample. The value for dry soil is taken at the beginning of the test, when the pressure cell is still dry and water hasn't been injected yet. The value for saturated soil is taken when the water has reached the edge of the column. The calibration is repeated for each experiment when the soil chamber is re-packed with a new soil sample.

Figure A- II shows the calibration curves of several couple of calibration points taken during different experiments. As shown in the chart, the calibration curves exhibit common patterns, assessing the consistency of the method.
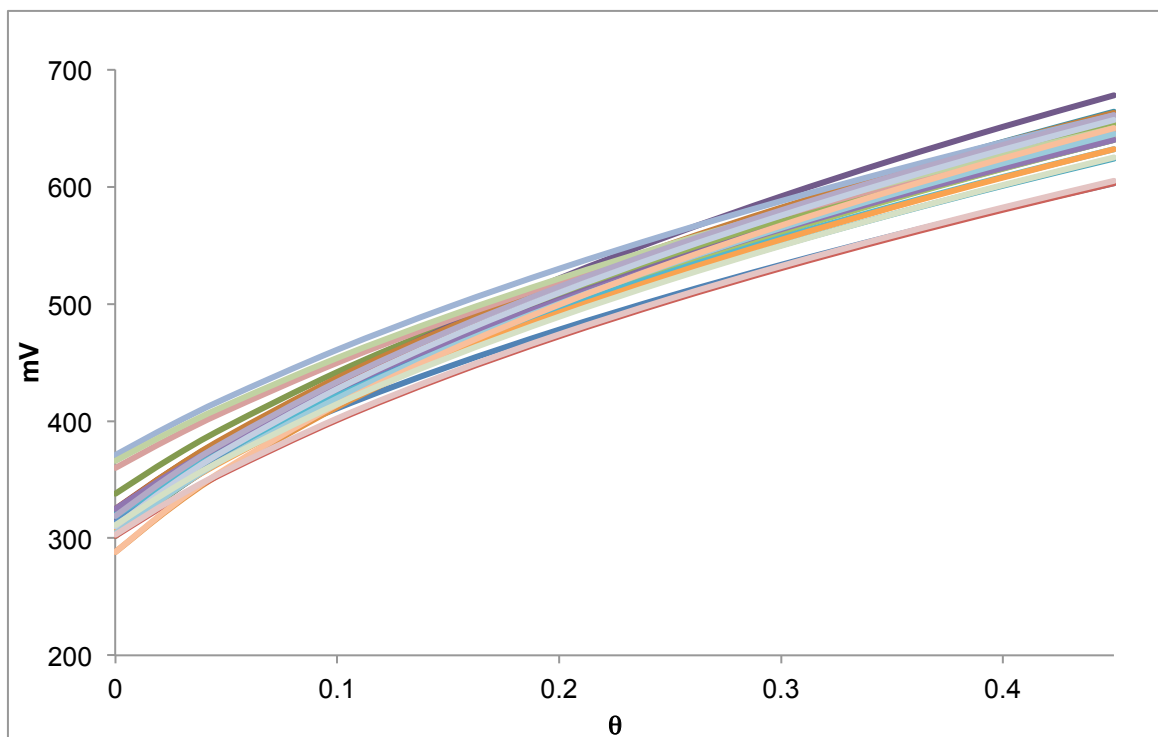

Figure A - II: Calibration curves of the EC-5s obtained from different calibration points.

Table A - II: Values for dry and saturated soil the three EC-5s (in mV) and their respective conversion in ADC^α ([mV]x1.3661)$^{2.5}$.

DRY SOIL VALUES						SATURADED SOIL VALUES					
mV			ADC1^a			mV			ADC1^a		
EC-5 1	EC-5 2	EC-5 3	EC-5 1	EC-5 2	EC-5 3	EC-5 1	EC-5 2	EC-5 3	EC-5 1	EC-5 2	EC-5 3
302	325	338	3457193	4153504	4581398	651	657	658	23586239	24133463	24225400
304	312	324	3514716	3750531	4121628	678	664	663	26108412	24781434	24688235
321	309	302	4026881	3661023	3457193	603	661	653	19475988	24502471	23767811
317	320	288	3902603	3995592	3070347	645	624	645	23046528	21216205	23046528
313	302	306	3780655	3457193	3572809	640	603	640	22602484	19475988	22602484
325	319	307	4153504	3964450	3602070	640	632	632	22602484	21902764	21902764
319	304	288	3964450	3514716	3070347	661	645	650	24502471	23046528	23495767
310	303	311	3690715	3485883	3720550	657	605	625	24133463	19637883	21301308

Appendix B: Results on Sand

Results on Sand

In this appendix are reported the results of the experiments that have been tested on the standard material, the coarse silica sand (Accusand C-190, Unimin Corp.), shown in Figure B- I, in order to verify the consistency of the methodology.

Figure B - I: Sample of coarse silica sand, Accusand C-190 (by Unimin Corp.), d50 = 0.73 mm, ρs = 2.66 g/cm³.

Saturated Hydraulic Conductivity

Chapter 3 describes the method used to measure the saturated hydraulic conductivity for the green roof growth media. Here are reported the results of the same methodology tested on sand. The experiment was repeated three times (each time with a different packing of the soil chamber) and the results are reported in Table B-I. In Figure B-II are shown the results of one of the three tests.

Table B-I: Results for the saturated hydraulic conductivity for three different experiments on silica sand.

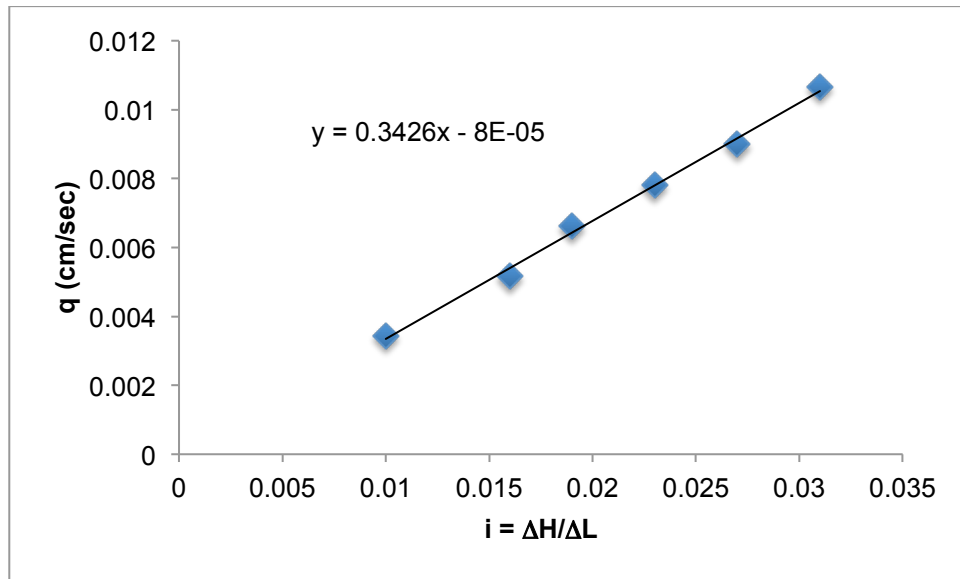| Trial #	Trial 1	Trial 2	Trial 3
K (cm/sec)	0.3340	0.3489	0.3426

Figure B-II: Saturated hydraulic conductivity (K, cm/sec) for silica sand.

There results are comparable with the hydraulic conductivity (for the same sand) reported in [78]. In the study is reported the intrinsic hydraulic permeability (k), which is equal to $k = 4.03*10^{-10}$ m^2. The saturated hydraulic conductivity can then be calculated with the following equation:

$$K = \frac{kg\rho_W}{\mu}$$

Where g represents the gravitational acceleration (9.81 m/s^2), ρ_W is the density of the water (0.99802 g/cm^3 at 21°C) and μ is the dynamic viscosity of the water (1.0002x10^{-3} Ns/m^2 at 20°C) [79]. With these values, the calculated hydraulic conductivity is K = 0.003496 m/sec = 0,3496 cm/sec which is comparable with the experimental results.

Thermal Properties

In Table III are reported the results of the thermal properties measured on the silica sand with the KD2 Pro using the two-needle probe SH-1 (described in Chapter 3). The thermal properties are measured for dry and saturated sand.

Table B-II: Thermal properties measured on dry and saturated sand.

	Thermal Conductivity, λ [W/mK]	Heat Capacity C_V, [MJ/m^{3}K]
Dry Sand	0.244	1.250
Saturated Sand	2.708	2.793

The values obtained for the silica sand (for the dry and saturated conditions) are comparable with the results reported in [80]. Indeed, the thermal conductivity for dry sand reported by [80], is between 0.25 and 0.30 W/mK and for saturated sand is approximately 2.75 W/mK. In the study the authors tested a similar type of silica sand with the same thermal properties analyzer KD2 Pro (using the two-needle probe SH-1). In the study the thermal properties were measured at different temperatures, however, the authors report that there are not temperature effects for dry and saturated conditions. Therefore, it is possible to compare the results obtained in the thesis (conducted at 20°C) with the values reported in [80]. Regarding the heat capacity the authors in [80] didn't report any values, however, in [78] the heat capacity reported for the same silica sand is 1.93 MJ/m^{3}K.

Appendix C: Incorrect Hydraulic Conductivity Results

As described in Chapter 3, two other experimental set-ups have been tested before the final configuration. The results and the problems occurred with these layouts are described in this appendix.

The first set-up consisted of measuring pressure head with three pressure transducers places along the length of the column or connected at the top and the bottom of the soil chamber. As described in Chapter 3, the pressure readings of the pressure transducers were not constantan over time or with the flow rate and the value of the calculated difference of head (ΔH) was not repeatable. As shown in Fig. C-I, every experiment gave different values of K and non-zero offset. For every experiment the pressure cell was packed with fresh soil that was flushed with carbon dioxide first, then saturated with D.I. water.
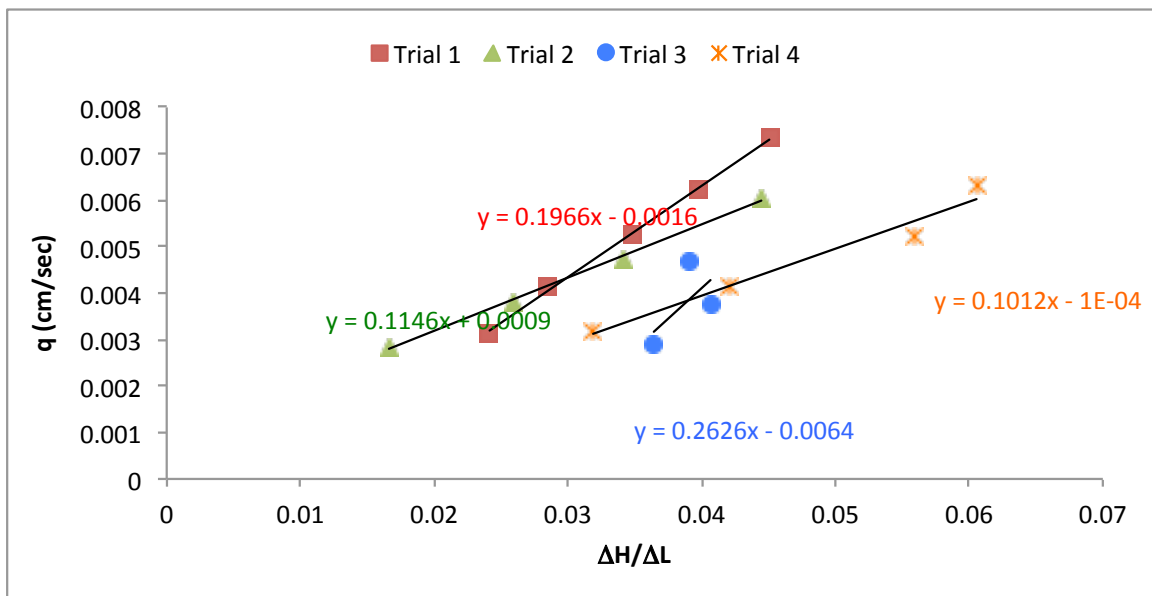

Figure C-I: Four experiments of saturated hydraulic conductivity using the first experimental set-up, where the pressure of the water to calculate the DH is measured with pressure transducers.

As described in Chapter 3, with the second experimental set-up, which consisted of the permeamiter and based on the ASTM method, the main problem, was that after few

flushes the soil specimen was classifying in layers an loosing compaction, giving an overestimated volumetric flow and not repeatable results of saturated hydraulic conductivity. In the following figure C-II are reported the results of three experiments.
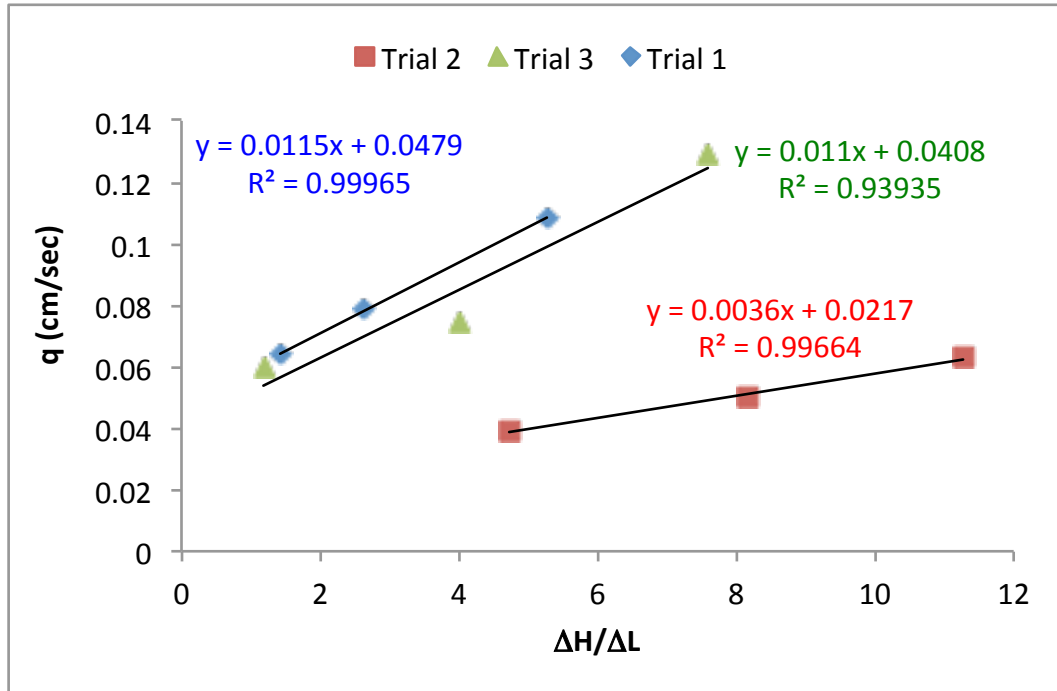

Figure C-II: Three experiments of saturated hydraulic conductivity using the second experimental set-up, based on the ASTM method.

Curriculum Vitae

Name: Ginevra Alessandra Perelli

Post-secondary   Politecnico di Milano
Education and   Milan, Italy
Degrees: 2008-2011 B.Sc.

Honors and
Awards: Double Degree Program 2012 (Milan, Italy)

Related Work   Teaching Assistant 2012-2014 (Western University,
Experience   London, CA)